THE UNIVERSITY OF
MELBOURNE

A tale of two (dark) fermions
Probing a dissipative hidden sector dark matter model

Sunny Vagnozzi
Supervised by Dr. Robert T. Foot

A thesis submitted in partial fulfilment of the requirements for the degree of Master of Science (Physics).

School of Physics
University of Melbourne
Australia

Abstract

The concept of a hidden sector, a set of additional particles and forces which interact with the Standard Model content predominantly via gravity, appears to be a promising approach towards accommodating dark matter without modifying the Standard Model. In this thesis we investigate a hidden sector featuring two Dirac fermions charged under an unbroken $U(1)'$ gauge symmetry. The associated gauge field, the dark photon, can interact via kinetic mixing with the ordinary photon. We explore the phenomenology of this model in three different areas: early Universe cosmology, from Big Bang Nucleosynthesis to the onset of large-scale structure formation; galactic structure, where we formulate a dynamical model for the dark matter halo which is consistent with observations; and finally direct detection experiments, where we examine a possible diurnal modulation signal. We find that the model can explain various observed features of spiral galaxies, such as the cored density profile and the Tully-Fisher relation. These analyses are used to set constraints on the parameter space of the model.

October 24, 2014

Statement of contributions

Chapter 1 is an original review of dark matter physics and hence of existing work. Chapters 2,3,4,5 and Appendix A contain the author's own work, with the exception of Chapter 3.1.4.[1] The work on which Chapters 2 and 3 are based has been submitted for publication in a paper [1], Chapter 4 is part of work in progress to be published shortly [2].

Acknowledgements

"There are more things in heaven and earth, Horatio,
Than are dreamt of in your philosophy."

William Shakespeare, *Hamlet*

"Dark matter is what my research team is looking for. No one knows what it is. There's more stuff out there in the universe than we can see, that's the point. We can see the stars and the galaxies and the things that shine, but for it all to hang together and not fly apart, there needs to be a lot more of it to make gravity work, you see. But no one can detect it. So there are lots of different research projects trying to find out what it is, and this is one of them. ... We think it's some kind of elementary particle. Something quite different from anything discovered so far. But the particles are very hard to detect."

Philip Pullman, *His Dark Materials*

"For the movement of composite bodies is, as we said, determined by that simple body which preponderates in the composition. These premises clearly give the conclusion that there is in nature some bodily substance other than the formations we know, prior to them all and more divine than they."

Aristotle, *On the Heavens*

---

[1]This section on elliptical galaxies is almost exclusively Robert's work, which derived from his insight and some discussion we shared while working on [1]. Given the context in which this work arose, and its flowing well with the rest of the thesis, we thought it was a good idea to add it.

Contents

CHAPTER 1

INTRODUCTION: THE DARK MATTER PROBLEM

There are matters we see, there are matters we don't, there are the brightest of photons, there are the darkest of photons, there was the age of ions, there was the age of atoms, there was the season of radiation, there was the season of matter, it was the spring of stardust, it was the winter of stars - and above all, the dark matter halo so yearned to cool that half the photons coming from a star's deathbed insisted on being transformed, for good or for evil, into dark matter particles.[1]

1.1 Evidence for dark matter

Poetic or arcane as they might sound, the lines above are describing the journey we will undertake in the following pages, in an attempt to shed light on one of the biggest problems in modern cosmology: the mystery of dark matter. Already in his cosmological treatise *On the Heavens* (dated 350 BC) Aristotle had come to the conclusion that there had to be some form of matter other than the one we experience, guiding the motion of celestial bodies in the Universe. Still, it was not until the 1930s that scientific evidence started accumulating and pointing convincingly towards the existence of this new form of matter. We now refer to this as "dark matter", in contrast to the luminous "baryonic matter", which is very well described by the Standard Model of particle physics.

It was the year 1933 when Franz Zwicky, a Swiss astronomer at Caltech, was examining the Coma Cluster, and employed the virial theorem to estimate the total mass present within the cluster itself. What he found was that the luminous matter could only account for a small percentage of the total cluster mass, the rest of which had to be invisible, and which he coined *dunkle materie* ("dark matter") [3]. Still, more convincing evidence appeared in the late 1960s, when Vera Rubin and Kent Ford determined the rotational velocity profiles of edge-on spiral galaxies to unprecedented accuracy. These were found to be, to very good approximation, flat far beyond the region where luminous matter was present, in stark contrast with the fall-off which would be inferred from Kepler's law [4].

Further compelling clues as to the existence of non-baryonic dark matter came hand in hand with the drastic advance in our understanding of cosmology in recent years. Presently, we acknowledge that dark matter is critical to explaining the structure of the acoustic peaks that appear in the anisotropy spectrum of the Cosmic Microwave Background (CMB) [5]. These are a fingerprint dating from the very early Universe when photons and baryons were tightly coupled in a photon-baryon fluid. The fluid in question oscillated within potential wells provided by pressureless dark matter overdensities, in what are referred to as acoustic oscillations (see e.g. [6]). These potential wells were critical for the subsequent growth of matter overdensities (the seeds for future galaxies and clusters) following matter-radiation equality, and hence for large-scale structure (LSS) formation. It is of vital importance that they be provided by a form of matter which is non-baryonic, so as to not share the oscillating

---

[1]The sharp reader will have noticed some similarity between these lines and the *incipit* of Charles Dickens' much celebrated work, *A tale of two cities*. Given the title of this thesis, such similarity is of course not a coincidence.

dynamics of the photon-baryon fluid. The "non-baryonic" part here is decisive. Non-luminous baryons, although dark, simply will not do.

Our current understanding of LSS formation also suggests that dark matter should be "cold", that is, non-relativistic at the onset of structure formation. In scenarios where LSS formation is driven by hot dark matter (e.g. Standard Model neutrinos), structure formation is suppressed below the so called free-streaming scale.[2] Warm dark matter, a component with properties intermediate to the aforementioned two, is not entirely excluded.

There are a number of other well documented observational evidences which attest a virtually inevitable need for dark matter, for instance gravitational lensing and microlensing experiments (see for example [8]), observations of the Lyman-α forest, and so forth. *En masse*, these evidences also indicate that dark matter amounts to $\approx 85\%$ of the matter budget of the Universe [9].[3] Observations also reveal that, at least in spiral galaxies, dark matter is distributed in the form of a roughly spherical halo, which extends far beyond the range of luminous matter and is responsible for the inferred flat rotation curves. For a more comprehensive review on dark matter, refer for instance to [10].

The composition of dark matter, on the other hand, remains a mystery. Although a collisionless cold dark matter (CDM) model appears to operate superbly on large scales, correctly reproducing LSS formation and the matter power spectrum, this framework as currently understood also presents a series of shortcomings on small scales. For instance, collisionless CDM simulations predict a cuspy dark matter halo profile [11], in spite of astrophysical observations indicating that the profile is rather cored or, anyhow, lower than what collisionless CDM would predict. In the literature, this is referred to as the *core-cusp problem* (see [12] for a review on the topic). These same numerical simulations predict an excess of subhalos in juxtaposition to the number of observed satellite galaxies in the Local Group, which is lower by about an order of magnitude. This dilemma has been dubbed the *missing satellite problem*, or alternatively the *dwarf galaxies problem* [13].

1.2 Dark matter candidates

The Standard Model of particle physics (SM hereafter) is arguably one of the greatest accomplishments of physics. Based on the framework of spontaneously broken gauge groups, the SM describes the non-gravitational interactions of particles exceptionally well up to and slightly beyond the electroweak scale (for a review on the SM, see e.g. [14]). And yet, a number of arguments suggest that the SM as we know it is incomplete. As is well known, among the shortcomings of the SM is the lack of a suitable dark matter candidate.[4] There are

---

[2]Furthermore, LSS formation in the presence of hot dark matter predicts a "top-down" structure formation process, with structure forming from fragmentation of superstructures known as Zeldovich pancakes into smaller systems [7]. This is in blatant contrast with the commonly accepted "bottom-up" structure formation paradigm, based on a hierarchical merging of smaller structures into ever-growing larger ones (galaxies, galaxy groups, clusters, superclusters, sheets, walls and filaments, up until the End of Greatness at a scale ~ 100 Mpc), which is supported by a variety of observations.

[3]On the other hand, the matter content accounts for $\approx 32\%$ of the energy budget of the Universe, the remaining $\approx 68\%$ being made up of "dark energy", which drives the accelerated expansion of the Universe.

[4]There are several other drawbacks associated with the SM. Although it is not within the jurisdiction of this thesis to discuss them, for completeness we will hereby provide a succint overview for the curious reader. While some of these flaws are in a sense methaphysical (e.g., "why is parity violated?" or "why are there exactly three generations of quarks and leptons?"), others are more pressing. For instance, the SM is unable to account for neutrino masses (inferred from neutrino flavour oscillations), the observed predominance of matter over antimatter (baryogenesis) and the presence of dark energy. The reader might also have heard that the SM cannot accommodate gravity and suffers from the "hierarchy problem". Without going into further detail, we would just like to point out that these are in fact not problems associated to the SM *per se*, but rather to the QFT framework itself and to "the SM plus new physics at some higher energy scale" respectively.

a number of attributes which a proper dark matter candidate should abide by: 1) stability on cosmological timescales, which can typically be attained by means of an appropriate symmetry; 2) being able to reproduce the correct relic abundance, $\Omega_{dm}h^2 \simeq 0.12$ [9], and 3) to be "cold" or at most "warm". We now present a brief overview of a series of dark matter candidates which are discussed copiously in the literature, prior to offering a novel approach to accommodating dark matter (that is, hidden sectors), which we will follow in this work. For a more comprehensive review on dark matter candidates refer for instance to [15]. The reader who is somewhat less familiar with the particle physics side of dark matter might find it befitting to read for instance [16] first.

1.2.1 The WIMP miracle

Without any doubt, the most popular dark matter candidate in the literature is that of a weakly interacting massive particle, better known as WIMP. WIMPs do not take part in electromagnetic or strong interactions, and the strength of their interactions with ordinary matter is assumed to be comparable to that of the weak force; indeed, the scenario where WIMPs couple to the $W^\pm$ or Z bosons at tree level is not an uncommon one. Historically, WIMPs first caught the interest of the physics community when it was realized that, for a particle χ whose relic abundance was determined by thermal freeze-out, with thermally averaged annihilation cross-section $\langle\sigma_{ann}v\rangle$, the relic abundance would roughly be given by:

$$\Omega_\chi h^2 \approx 0.1 \left(\frac{\langle\sigma_{ann}v\rangle}{3 \times 10^{-26} \text{ cm}^3\text{s}^{-1}}\right)^{-1} . \tag{1.1}$$

For a particle χ with mass at the electroweak scale (100 GeV-few TeV), exhibiting interactions of strength comparable to the weak one, the thermally averaged annihilation cross-section turns out to be in the ballpark, $\sim 10^{-26}$ cm^{3}s^{-1}. This feature is referred to as the "WIMP miracle", and is unquestionably the reason behind the great popularity of WIMPs among physicists. In addition, WIMPs appear frequently in theories beyond the Standard Model, such as Supersymmetry (SUSY, for a review see for instance [17]). In SUSY, the introduction of a supplementary $\mathbb{Z}_2$ symmetry known as R-parity implies that the lightest supersymmetric partner is stable, making it a good dark matter candidate [18].[5]

1.2.2 Exotics

A different class of dark matter candidates are referred to as "exotics". These customarily originate through non-thermal effects, such as phase transitions. An example of such candidate is the axion, first proposed by Peccei and Quinn to solve the strong CP problem (that is, the apparent lack of CP violations in the strong interaction, which follows from very tight bounds on the neutron dipole moment) [19]. Peccei and Quinn introduced an additional $U(1)$ symmetry, the Peccei-Quinn symmetry, which is broken at some energy scale; the pseudo Nambu-Goldstone boson associated with the breaking of this symmetry is the axion. Further examples of exotic dark matter candidates include WIMPzillas, cryptons, brane world dark matter, Q-balls, CHAMPs, D-matter, and so forth, with a list that could proceed *ad infinitum*.

1.2.3 Astrophysical candidates

To conclude, there also are a number of dark matter candidates motivated by astrophysics. The preeminent one is that of Massive Astrophysical Compact Halo Objects (MACHOs), which describe any type of astronomical body composed of baryonic matter which does

---

[5]Hopefully SUSY fans out there will not be offended, but I personally find this somewhat *ad hoc*.

not emit radiation and meanders through the interstellar space (e.g. primordial black holes, brown dwarfs, neutron stars, white dwarfs, unassociated planets, and so forth). At present, MACHOs are almost entirely ruled out as an explanation for dark matter primarily on the basis that they are composed of non-luminous but baryonic matter nonetheless. *Ergo*, they cannot account for the non-baryonic matter content which appears necessary to explain the CMB anisotropy spectrum.

1.3   A hidden sector approach

As we have seen, a profusion of dark matter candidates emerge from the most disparate scenarios, some of which originate from well motivated particle physics theories, other which arise as solutions to problems which had nothing to do with dark matter. Nevertheless, finding a way of systematically incorporating dark matter candidates, instead of having to rely on theories which by a rather fortunate chance happen to have one, would be somewhat appealing. From a particle physics mindset, a viable avenue for accommodating dark matter is by extending the SM to include a hidden sector (HS). In other words, an extra sector encompassing new particles and new forces which interact with the SM content primarily via gravity. This implies the particle content of the hidden sector being naturally "dark". The dynamics of the particles and interactions in the two sectors are described by the Lagrangian:

$$\mathcal{L} = \mathcal{L}_{\mathrm{SM}} + \mathcal{L}_{\mathrm{HS}} + \mathcal{L}_{\mathrm{mix}} \, , \tag{1.2}$$

where $\mathcal{L}_{\mathrm{SM}}$ and $\mathcal{L}_{\mathrm{HS}}$ are the SM and HS Lagrangians respectively, and $\mathcal{L}_{\mathrm{mix}}$ comprises possible additional non-gravitational interactions which couple the two sectors. The HS Lagrangian, $\mathcal{L}_{\mathrm{HS}}$, exhibits a $\mathcal{G}'$ gauge symmetry, with the associated gauge fields mediating the interactions between particles in the HS.

In the HS, accidental global or discrete symmetries could arise. If that occurs, the lightest degree of freedom charged under either one of these accidental symmetries, or the gauge symmetry $\mathcal{G}'$ itself, is stable, thus providing a potential dark matter candidate. The dark matter structure that follows can be extremely rich, comprising self-interactions (possibly dissipative), formation of bound states, novel experimental signatures, and so forth. The reader will have realized that the dark matter phenomenology of this model is closely linked to the particle physics underlying the HS, that is, the particle and gauge bosons content of the HS.

Consider the simple possibility where $\mathcal{G}'$ contains a $U(1)$ group as a factor. In this case, a dark version of quantum electrodynamics is expected to arise, with interactions which are mediated by a dark photon. The dark photon can mix with the ordinary photon via a kinetic mixing interaction, to which we will devote further and more extensive discussions in Chapter 1.3.1. Early work on a possible dark electromagnetic sector was carried out in [20]. The idea was reconsidered some years later in [21], where it was pointed out that dark matter stability might be due to a conservation law following from a hidden gauge symmetry.

Let us consider the possibility of $\mathcal{G}'$ containing a $U(1)$ factor further. This choice still leaves quite a bit of leeway with respect to the possible phenomenology. For instance, the symmetry could be broken (as explored recently in e.g. [22]), following which the dark photon acquires a mass, or unbroken (as in e.g. [23–26]), which implies the dark photon is massless. In the former case, if the mass of the dark photon is sufficiently high, the phenomenology of such model might be indistinguishable from that of WIMPs. In the latter, the masslessness of the dark photon implies the presence of long range Coulomb-like interactions, which can lead to dissipative dynamics. These entail energy loss on a timescale which is significantly less than the Hubble time.

Even when dissipative interactions can potentially arise, one can reside in the region of parameter space where dark matter is atomic and hence collisional, but not dissipative. One collision per Hubble time can be sufficient to avoid significative dissipation, while at the same time possibly allowing to address some of the shortcomings of collisionless CDM on small scales [27]. On the other hand, even if dark matter were non-atomic and hence ionized, a considerate (but certainly restricted) choice of parameters can still lead to a non-dissipative plasma, although no significative work has been done in this direction.

In the presence of significative dissipative interactions one can make two final choices. In the first, only a subdominant component of the dark sector exhibits dissipative dynamics. This is the case for instance of double-disk dark matter, a case considered in the very recent literature. In this model, the dissipative interactions allow for this dark matter component to cool efficiently and form a disk rather than a halo [28]. The alternative choice instead consists in having the entire dark sector being subject to dissipative dynamics: in this case, the need for a heat source which can replace the energy lost is inescapable. Else, the dissipative interactions are expected to allow the dark matter halo to cool on a timescale much less than the Hubble time, which would be in stark contrast with observations.

The choice of the entire hidden sector featuring significative dissipative interactions, and hence requiring a heat source, is largely unexplored in the literature. The only exception is possibly mirror dark matter, a very particular model which we discuss in the next section. In this thesis we consider what is arguably the simplest model featuring a dissipative dark sector. The position occupied by our model in the landscape of possible hidden sectors is given in the diagram below.

Hidden sector gauge symmetry $\mathcal{G}'$

$\mathcal{G}' \not\supset U(1)$ $\mathcal{G}' \supset U(1)$

$U(1)$ broken $U(1)$ unbroken

Non dissipative   Dissipative

No heat source   Heat source

Our model
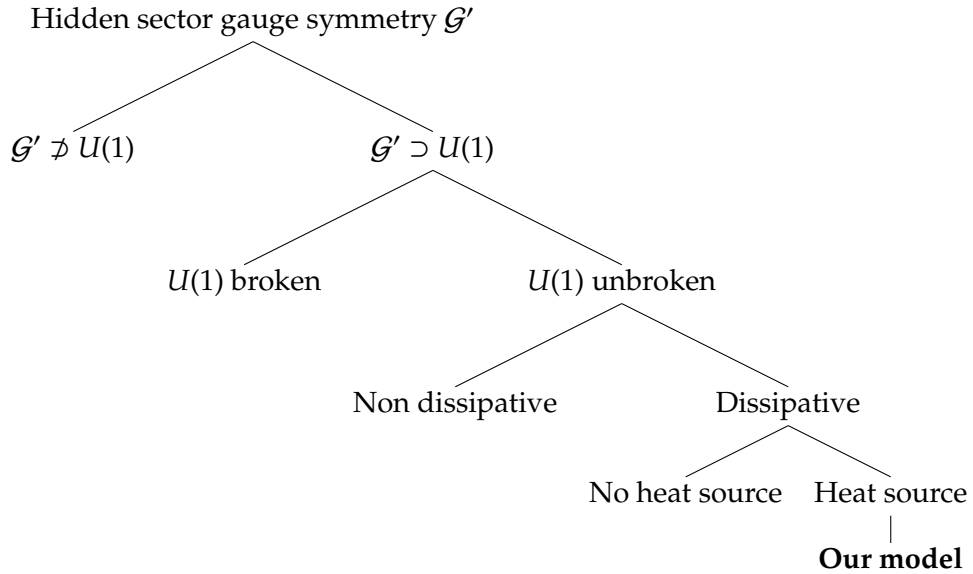
1.3.1 Mirror dark matter

Mirror dark matter (MDM henceforth) is a notable example of a HS model, with the HS being exactly isomorphic to the SM (including couplings). It follows that each SM particle and gauge field is now mapped, via an exact $\mathbb{Z}_2$ symmetry, to a mirror partner [29]. Although MDM has the potential to act as a suitable dark matter candidate, the reason for which it was first studied in detail was actually that of addressing the issue of the observed parity violation in nature. If the aforementioned $\mathbb{Z}_2$ symmetry, along with switching SM particles with their mirror partners, additionally swaps left and right chiral fields, it can be interpreted as parity. In the MDM framework parity emerges as a fundamental unbroken symmetry of the theory, which appears to be broken for the sole reason that we are not able to detect

mirror particles. For an up-to-date and comprehensive review on MDM refer to [30].

In addition to the SM and mirror sectors, Lagrangian terms which couple the two are allowed, provided they are gauge-invariant and renormalizable.[6] As it turns out, there are only two such terms one can write: the first is a Higgs-mirror Higgs quartic coupling, which is not expected to play a salient role in our discussion; a second and far more important term, with extremely fascinating astrophysical and cosmological consequences, is a kinetic mixing term, which mixes the ordinary and mirror photons (with field-strength tensors $F_{\mu\nu}$ and $F'_{\mu\nu}$ respectively):[7]

$$\mathcal{L}_{\text{km}} = \frac{\epsilon}{2} F^{\mu\nu} F'_{\mu\nu} \, . \tag{1.3}$$

What is the physical effect of this term? The trick here [32] is to perform a non-orthogonal transformation on the photon and mirror photon gauge fields (A_μ and A'_μ), which results in two massless unmixed states. From here one can easily rotate into a basis where only one of these two states couples both to SM and mirror particles, while the other only couples to mirror particles: the former is then identified as being the physical photon, and the latter as the mirror photon.[8] In a basis suitable to an ordinary matter environment, the coupling of the physical photon to SM particles with charge Q is Qe (as one would expect), while the coupling to mirror particles with mirror charge Q' is $\epsilon Q'e$ [30, 32]. Given that the requirement $\epsilon \ll 1$ is determined *a posteriori*, these particles are commonly referred to as millicharged particles.

It has been shown that on large scales the phenomenology of MDM can be *de facto* indistinguishable from that of collisionless CDM, reproducing the successful LSS formation scenario. This is possible provided that suitable initial conditions are satisfied [33, 34] and that the kinetic mixing parameter, ϵ, satisfies the bound $\epsilon \lesssim \text{few} \times 10^{-9}$ [30, 35]. Under these conditions, MDM behaves cosmologically as collisionless CDM following matter-radiation equality.

In constrast, the physics of MDM is very different from that of collisionless CDM on small scales, featuring a much richer array of interactions and nontrivial dynamics, particularly in the context of galactic structure. In the MDM framework it is assumed that the dark matter halo is in the form of a roughly spherical plasma, which can cool at a rate Γ_{cool} via dissipative interactions, such as thermal bremsstrahlung. It is estimated that the halo cooling timescale is of order 3×10^8 years, an issue which is referred to as the *radiative cooling problem* [36]. In order to account for the observed sphericity of the dark matter halo, a sizeable heat source which can replace the energy lost to dissipation is required.

It has been extensively argued in the MDM framework that an adequate heat source can arise from ordinary core-collapse supernovae [36]. The proposed mechanism invokes kinetic mixing induced processes in the core of the supernovae (e.g. $e\bar{e} \to e'\bar{e}'$, $\gamma \to e'\bar{e}'$). For $\epsilon \sim 10^{-9}$, these processes are expected to convert $\sim 1/2$ of the core-collapse energy into light mirror particles: initially predominantly mirror electron pairs, which are ultimately reprocessed into mirror photons in the region surrounding the supernovae (see e.g. [37]). These mirror

---

[6]A simple criterion to determine whether a Lagrangian term is renormalizable is to verify whether the mass dimension of the relevant coupling is nonnegative.

[7]In early works it was usually assumed that such a term arised at loop level, provided a connector particle existed. In 1991 Foot and He reiterated once and for all that, as the kinetic mixing term is renormalizable and gauge invariant, it can legitimately be present as a Lagrangian term [31].

[8]One might question how did this asymmetry arise, given that we started with a Lagrangian which is perfectly symmetrical upon interchange of ordinary and mirror states. Of course, the broken symmetry is only apparent, and is the result of a transformation which is appropriate within an environment dominated by visible matter. In fact, one can make a different choice of transformation, which leads to a mirror photon coupling both to mirror and SM particles, and a sterile photon coupling only to SM particles. At the end of the day, this is only a choice of basis, which does not affect any physical result (see [30] for further discussions).

photons can heat the halo at a rate Γ_{heat} through a variety of avenues. It is argued that the preeminent process is photoionization of a mirror metal component (e.g. mirror oxygen, mirror iron). This is possible since, for the range of halo temperatures considered, these mirror metal components retain their K-shell mirror electrons.

Furthermore, it is pointed out that a variety of feedback mechanisms can dynamically modify the quantity $\Gamma_{\mathrm{heat}} - \Gamma_{\mathrm{cool}}$, until the equilibrium situation $\Gamma_{\mathrm{heat}} = \Gamma_{\mathrm{cool}}$ is reached, without having to invoke fine tuning between the two rates. More in-depth studies of MDM in the context of galactic structure have demonstrated that this framework is also able to provide an explanation to a series of observational properties of spiral galaxies which arise, to a greater or lesser extent, as a consequence of the aforementioned energy balance relation, $\Gamma_{\mathrm{heat}} = \Gamma_{\mathrm{cool}}$ [38]. To conclude, MDM has also been shown capable of explaining the results, both positive and negative, from the dark matter direct detection experiments (DDEs henceforth), alleviating the apparent tension between some of them [30, 39].

1.3.2 Two-component hidden sector dark matter

Mirror dark matter, while representing a suitable and well motivated example of a HS dark matter candidate, is certainly a very restricted one: the complete isomorphism between the visible and mirror sectors implies all couplings being equal. It follows that MDM possesses only two free parameters: the kinetic mixing and Higgs-mirror Higgs quartic interactions couplings. Nevertheless, there exist alternative models which have a similar phenomenology to MDM while at the same time being far less restrictive. Recall the salient features inherent to MDM which are at the origin of its peculiar phenomenology: an unbroken $U(1)$ interaction (mirror electromagnetism, the mirror photon being kinetically mixed with the ordinary photon), implying significant dissipative dynamics in the HS and hence the need for a heat source.

An example of such an alternative model is that of a two-component HS featuring two particles, hereafter denoted by F_1 and F_2, charged under an unbroken $U(1)$ gauge symmetry; the relevant interactions are mediated by a massless dark photon, which can interact via kinetic mixing with the ordinary photon. Such a model is obviously closely related to others discussed in the recent literature, which feature a dark electron and a dark proton [22–26]. In addition, given that the massless dark photon mediates long-range dissipative interactions, the phenomenology of this model closely resembles that of MDM, with the ligher particle corresponding to the mirror electron and the heavier one to mirror nuclei. As we will discuss more thoroughly in Chapter 2, the relic abundances of the two particle species are determined by a particle-antiparticle asymmetry. That is, the model is an example of *asymmetric dark matter*, extensively discussed in the recent literature (see e.g. [40, 41] for reviews on the topic).[9] In addition, this framework has been analysed in recent years in the context of DDEs, and has been proved to be capable of explaining the results arising from the various experiments consistently provided one particle be much heavier than the other and the kinetic mixing parameter, ϵ, satisfies $\epsilon \sim 10^{-9}$ [43].[10]

---

[9]Asymmetric dark matter is very well motivated on the basis of the observation that $\Omega_{\mathrm{dm}}/\Omega_{\mathrm{b}} \simeq 5$, that is, that dark and visible matter have similar relic abundances. Given that the relic abundance of visible matter is largely determined by the baryon-antibaryon asymmetry (baryogenesis), one might speculate that the relic abundance in the dark sector might also be determined by a particle-antiparticle asymmetry. Moreover, in several asymmetric dark matter scenarios, dark matter and visible matter share a common origin (as for instance in the case of "pangenesis" [42]).

[10]The recent results from the LUX experiment [44] call for a reconsideration of this explanation. We will provide more food for thought in this respect in Chapter 4.3.

Outline of research project

The two-component hidden sector dark matter model described above has been explored in detail only with respect to direct detection experiments. The aim of our research project is to scrutinize its phenomenology in a number of other contexts, to verify whether it can indeed provide a suitable dark matter candidate. In Chapter 2 we analyse the model's early Universe phenomenology, focusing on two main areas: the addition of extra energy density during the radiation dominated era, in particular at the epochs of Big Bang Nucleosynthesis (BBN) and Hydrogen recombination; and the physics of dark recombination, during which the charged dark particles combine into neutral dark states. In Chapter 3, we probe this model in the field of galactic structure, and find that it can explain a number of puzzling observational properties of spiral galaxies. In Chapter 4 we expound some experimental signatures of the model, and in particular argue that its self-interacting nature is expected to lead to a diurnal modulation signal, particularly enhanced for direct detection experiments located in the Southern hemisphere. Finally, in Chapter 5 we draw a few closing remarks. For further details, we redirect the reader to our paper, on which the work carried out in Chapters 2 and 3 is based [1].

CHAPTER 2

EARLY UNIVERSE COSMOLOGY

As discussed earlier, a viable and well motivated way of incorporating dark matter is by means of a hidden sector. We now begin our analysis of the explicit HS outlined in the previous Chapter. That is, a HS featuring an unbroken $U(1)'$ symmetry, whose interactions are mediated by a massless gauge boson, the *dark photon* (γ_D). The HS additionally encompasses two stable dark matter particles, F_1 and F_2, taken to be Dirac fermions, with masses m_{F_1} and m_{F_2}. The two particles are charged under the $U(1)'$ gauge symmetry, with charges Q'_{F_1} and Q'_{F_2}. We will assume the charges are opposite in sign, although not necessarily the same in magnitude, with charge ratio $Z' \equiv Q'_{F_2}/Q'_{F_1}$.

In the early Universe, dark electromagnetic interactions are expected to efficiently annihilate the symmetric components of the F_j abundances. *Ipso facto*, our model is an example of *asymmetric dark matter*, that is, one where the dark matter abundance is set by a particle-antiparticle asymmetry (refer for instance to [40, 41]). Without loss of generality, we can assume that the HS today contains negligible amounts of dark matter antiparticles: $\overline{F}_1$ and $\overline{F}_2$. Defining n_{F_j} to be the number density of the F_j particle, local neutrality of the Universe jointly with dark matter asymmetry then imply that $n_{F_1}Q'_{F_1} + n_{F_2}Q'_{F_2} = 0$.

We now proceed to write down the Lagrangian of our model. Apart from the kinetic terms for the dark photon and dark fermions, and the mass term for the latter, the only other renormalizable and gauge-invariant term we can write is a kinetic mixing one, that is, one that couples the ordinary photon to the dark photon [31]. The Lagrangian is:

$$\mathcal{L} = \mathcal{L}_{\text{SM}} - \frac{1}{4}F'^{\mu\nu}F'_{\mu\nu} + \overline{F}_1(iD_\mu\gamma^\mu - m_{F_1})F_1 + \overline{F}_2(iD_\mu\gamma^\mu - m_{F_2})F_2 - \frac{\epsilon'}{2}F^{\mu\nu}F'_{\mu\nu}\,, \tag{2.1}$$

where $F'_{\mu\nu} = \partial_\mu A'_\nu - \partial_\nu A'_\mu$ is the field-strength tensor for the dark electromagnetic interaction, whose mediator, the dark photon, is described by the gauge field A'_μ.[1] The dark fermions are instead characterized by the quantum fields F_j, and the covariant derivative relevant to the dark electromagnetic interaction is $D_\mu F_j = \partial_\mu F_j + ig'Q'_{F_j}A'_\mu F_j$, with g' being the coupling. Note here how two accidental $U(1)$ symmetries arise and imply conservation of F_1 and F_2 number, and hence stability of our dark matter particles. As we mentioned in Chapter 1, this is quite a general feature of hidden sectors, perhaps explaining their appeal to the eyes of phenomenologists: the predicted spectrum of dark matter particles can easily be made massive, dark and stable. A good dark matter candidate indeed![2]

It will be useful to define the dark fine structure constant, which characterizes the strength of the interactions of F_1 with the dark photon: $\alpha' \equiv (g'Q'_{F_1})^2/4\pi$. The coupling of F_2 with the dark photon will instead be described by $Z'\alpha'$, where recall Z' is the charge ratio of F_2 to F_1.

---

[1] Here $F_{\mu\nu} = \partial_\mu A_\nu - \partial_\nu A_\mu$ is the field-strength tensor for the electromagnetic interaction [$U(1)_Q$], mediated by the photon, which is described by the gauge field A_μ.

[2] One could consider a similar two-component hidden sector model charged under an unbroken $U(1)'$ interaction where the two dark matter particles are bosons instead. All the considerations we make in this subsection will hold (e.g., stability of the two dark matter particles as a consequence of two accidental symmetries, and so forth), and the bounds which we will derive in this work and summarize in Chapter 3.3 will be valid up to factors of order unity, which account for spin statistics. Nevertheless, for the sole purpose of definiteness, in this work we focus on the fermionic model.

As we have seen in the previous Chapter, the physical effect of kinetic mixing is to endow the dark fermions with ordinary electric charge:

$$g' Q'_{F_j} \epsilon' \equiv \epsilon_{F_j} e \,. \tag{2.2}$$

Note that $\epsilon_{F_2} = Z' \epsilon_{F_1}$, and hence the two are not simultaneously independent parameters: we choose by convention $\epsilon \equiv \epsilon_{F_1}$ to be the independent one. Note at this point that the fundamental physics of our dark matter model is described by five independent parameters: $m_{F_1}, m_{F_2}, \alpha', \epsilon$ and Z'. For definiteness we will examine the region of parameter space where $m_{F_1} \ll m_{F_2}$ and Z' is an integer.

While our model is of course UV complete and renormalizable, it is also possible for it to be the low energy effective field theory limit of a more complete framework. If, for instance, such a framework features a confining interaction (which could possibly arise, for example, from an $SU(3)'$ symmetry), then F_1 and/or F_2 might represent bound states whose mass originates from the dark confinement scale (as occurs for instance in [45]).[3] Another possibility is that the mass terms for F_1 and F_2 might arise from a hidden sector scalar, H', with non-zero vacuum expectation value ($\langle H' \rangle \neq 0$), via a Lagrangian term such as $\lambda_j H' \overline{F}_j F_j$ (this is of course reminiscent of how the masses of quarks and leptons originate in the SM).

Let us briefly recall where our model sits in the landscape of hidden sectors (which is well depicted by the tree diagram on page 10). The massless dark photon mediates long-range dissipative interactions, and hence the galactic dark matter halo is expected to cool via these dissipative processes (e.g. thermal dark bremsstrahlung). Inevitably, we incur in the need for a heat source which can replenish the HS with the energy lost to dissipation. Unlike the other models depicted in the diagram, here a pivotal role is that played by kinetic mixing. We will call on kinetic mixing induced processes within the core of ordinary supernovae to replace the energy lost to dissipative interactions. The proposed mechanism involves at first F_1-$\overline{F}_1$ pair production (recall F_1 is the lightest of the two fermions), eventually annihilating into dark photons which can escape and heat the halo. This is possible if $\epsilon \sim 10^{-9}$ and $m_{F_1} \lesssim$ few $\times\, T_{\mathrm{SN}} \simeq 100$ MeV, where $T_{\mathrm{SN}} \simeq 30$ MeV is the maximum temperature that is reached in the core of ordinary supernovae. At the same time, we obtain a lower limit on m_{F_1} from studies of White Dwarfs [46, 47] and Red Giants [48]: $m_{F_1} \gtrsim 0.01$ MeV (see for instance [49, 50] for more recent summaries of the bounds). These limits define the range of parameter space we will analyse in this work.

One final comment before we proceed. Although it is required of the kinetic mixing parameter to be small ($\epsilon \sim 10^{-9}$, as we will confirm in the course of this work), this does not represent a problem such as radiative instability. In fact, generally speaking, in theories with hidden sectors small values for the mixing couplings are technically natural,[4] an idea which is known as Poincaré protection [51]. In the limit $\epsilon \to 0$, the symmetry of the theory is enhanced to $\mathcal{G}_P^{\mathrm{SM}} \otimes \mathcal{G}_P^{\mathrm{HS}}$, where $\mathcal{G}_P$ denotes the Poincaré group. In other words, one can perform independent Poincaré transformations on the SM and hidden sectors, while this would not be possible in presence of mixing between the two.

2.1   Evolution of T_{γ_D}/T_γ

Outfitted with all the required tools, we now begin by examining the phenomenology of this model in the early Universe, during the course of the radiation dominated era. At this time, successful early Universe cosmology sets tight bounds on the contributions of new physics to

---

[3]Compare this case with how the proton mass arises from the Λ_{QCD} scale in the Standard Model.

[4]In the sense of 't Hooft, that is, a parameter is naturally small if in the limit of the parameter being set to zero, the symmetry of the theory is increased.

the energy density. This comes about because processes that take place in the early Universe, chief among them BBN and the formation of the CMB, are extremely sensitive to the energy density at that time. For instance, small modifications in the energy density could result in changes in the predicted Helium fraction or the form of the CMB anisotropy spectrum.

Let us define the temperatures of the photon and dark photon to be T_γ and T_{γ_D} respectively. The essence of the above discussion is that successful early Universe cosmology requires $\mathcal{X} \equiv T_{\gamma_D}/T_\gamma \ll 1$ to hold at some early time. How early? It is at most necessary to require $\mathcal{X} \ll 1$ at, for instance, the QCD phase transition (QCDPT), which occured when the temperature of the visible sector was $T_\gamma \sim 100$ MeV. Even if $\mathcal{X} \sim 1$ did hold prior to the QCDPT, the heating of the visible sector which ensued from the QCDPT would have been ample to establish $\mathcal{X} \ll 1$ subsequently. There exist alternative ways by means of which one can achieve such initial condition ($\mathcal{X} \ll 1$) prior still to the QCDPT. For instance, within inflationary models, asymmetric reheating is a possibility which has been discussed to a great extent in the literature (see for example [52–54]).

As discussed previously, kinetic mixing bestows the dark particles with a tiny ordinary electric charge, allowing them to couple to the visible photon and hence to ordinary matter, albeit very weakly.[5] Therefore, even if the Universe did begin with $\mathcal{X} = T_{\gamma_D}/T_\gamma \simeq 0$, T_{γ_D} would be generated by way of kinetic mixing induced processes, which transfer energy and entropy between the visible and dark sectors. We shall now study the evolution of $\mathcal{X}$, subject to the initial condition $\mathcal{X} \simeq 0$. This quantity is useful in evaluating the contribution of new physics to the energy density in the early Universe, and hence will allow us to set bounds on the available parameter space.

A note of caution is needed here: although the region of parameter space 0.01 MeV $\lesssim m_{F_1} \lesssim 0.1$ MeV is certainly allowed , here we will focus exclusively on the range 0.1 MeV $\lesssim m_{F_1} \lesssim 100$ MeV. The reason is that within the region 0.01 MeV $\lesssim m_{F_1} \lesssim 0.1$ MeV, a series of complications arise, both in the context of early Universe cosmology and galactic structure, which time (and certainly not a lack of curiosity) did not allow us to consider. The issue of dealing with the complications which arise in this region of parameter space is left for future work.

We commence by considering the processes which allow for energy and entropy transfer between the visible and dark sectors. Among these channels, to order ϵ^2, we find $e\bar{e} \to F_j\bar{F}_j$, $eF_j \to eF_j$, $\gamma\gamma_D \to F_j\bar{F}_j$, $\gamma F_j \to \gamma_D F_j$, $\gamma \to F_j\bar{F}_j$ (plasmon decay), and so forth. If F_2 is significantly heavier than F_1 [more specifically, if $m_{F_2} \gg Z'^2 \max(m_e, m_{F_1})$, where $m_e \simeq 0.511$ MeV is the electron mass], we can safely neglect processes involving F_2. Plasmon decay is expected to be important only for $m_{F_1} \lesssim \omega_P/2$, where $\omega_p = \sqrt{4\pi\alpha T^2/9}$ is the plasma frequency (see e.g. [50]). During the period of interest (from BBN to the formation of the CMB) plasmon decay is only important for $m_{F_1} \lesssim 50$ keV, which is out of the range we are considering, as discussed above. Finally, of the remaining processes, we expect $e\bar{e} \to F_1\bar{F}_1$ to dominate, since the rates for the other processes are suppressed by a factor $\sim n_{F_1}/n_e \sim (T_{\gamma_D}/T_\gamma)^3$ and, as we will show later in our work, we are typically constrained to reside in the region of parameter space for which $(T_{\gamma_D}/T_\gamma)^3 \ll 1$.[6]

The treatment that follows will be a generalization of the more specific MDM case analysed in [35], from which we will draw extensively, and which itself followed earlier works [34, 50, 56]. The cross-section for the s-channel process $e\bar{e} \to F_1\bar{F}_1$ is analogous to that of

---

[5]The term "weak" here has nothing to do with the weak force, but refers exclusively to the coupling being minuscule.

[6]While we were working on this thesis and on [1], the paper [55] which performed a similar analysis with the inclusion of other channels appeared. As shown there, the net result of these extra channels is to strengthen the bounds we will obtain by a factor of $\lesssim 2$. Nonetheless, it is worth pointing out that the bounds arising from dark recombination, to be discussed in Chapter 2.3.3, are more stringent than the ones we will obtain here.
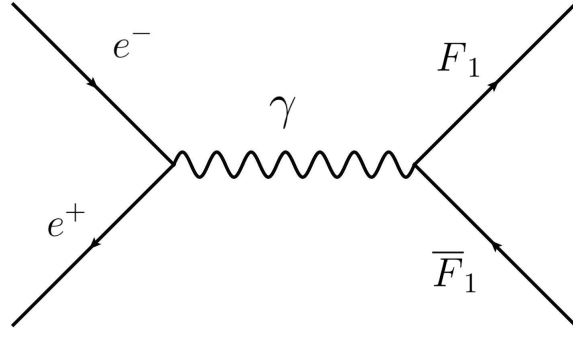
Figure 2.1: Feynman diagram for the process $e\bar{e} \to F_1\bar{F}_1$.

muon pair production, with the prime difference consisting in the coupling of F_1 to the ordinary photon being given by ϵe. The cross-section for this process (with Feynman diagram depicted in Figure 2.1[7]) is:

$$\sigma = \frac{4\pi}{3s^3}\epsilon^2\alpha^2 \sqrt{\frac{s - 4m_{F_1}^2}{s - 4m_e^2}}(s^2 + 2(m_e^2 + m_{F_1}^2)s + 4m_e^2 m_{F_1}^2) \, , \tag{2.3}$$

where $\sqrt{s}$ is the center-of-mass-energy, $\alpha \equiv e^2/4\pi$ the fine-structure constant and m_e the electron mass. Designating by R the scale factor, the process above allows for energy transfer between the visible and dark sectors within a comoving volume R^3 at a rate:

$$\frac{dQ}{dt} = R^3 n_e n_{\bar{e}} \langle \sigma v_{\text{Møl}} \mathcal{E} \rangle \, , \tag{2.4}$$

where $\langle \sigma v_{\text{Møl}} \rangle$ is the relevant thermally averaged cross-section, $\mathcal{E}$ is the total energy of the system and the electron and positron number densities can be found in e.g. [58]:

$$n_e \simeq n_{\bar{e}} = \frac{1}{\pi^2} \int_{m_e}^{\infty} dE \, \frac{\sqrt{E^2 - m_e^2}E}{1 + e^{\frac{E}{T_\gamma}}} \, . \tag{2.5}$$

In order to evaluate $\langle \sigma v_{\text{Møl}} \mathcal{E} \rangle$, we will trace the steps of [34, 59]. By replacing the exact Fermi-Dirac distribution with a simpler Maxwellian one, laborious algebra, which we shall not display here[8], gives us the end result:

$$\langle \sigma v_{\text{Møl}} \mathcal{E} \rangle = \frac{\omega}{8m_e^4 T_\gamma^2 [K_2(\frac{m_e}{T_\gamma})]^2} \int_{4\mathcal{M}^2}^{\infty} ds \, \sigma(s - 4m_e^2) \sqrt{s} \int_{\sqrt{s}}^{\infty} dE_+ \, e^{-\frac{E_+}{T_\gamma}} E_+ \sqrt{\frac{E_+^2}{s} - 1} \, , \tag{2.6}$$

where $\omega \approx 0.8$ accounts for a number of approximations, such as the replacement of the actual Fermi-Dirac distibution with the simpler Maxwell-Boltzmann one [34]. $K_2(z)$ is the modified Bessel function of the second kind and argument z, and $\mathcal{M} \equiv \max(m_e, m_{F_1})$.

Given that the rates of self-interaction processes are bigger than the kinetic mixing induced ones by many orders of magnitude ($\sim 1/\epsilon^2$), we can model the early Universe as comprising two subsystems exchanging energy while remaining instantaneously in thermodynamical equilibrium: the visible sector, at a temperature T_γ, and the dark sector, at a temperature T_{γ_D}. The conditions required to apply the second law of thermodynamics are thus met. In principle we would have to take the neutrino subsystem (at a temperature

---

[7]Feynman diagram was drawn using *Jaxodraw* [57].

[8]This is a fairly standard result, widely used in high energy physics and cosmology. For the pure pleasure of doing long calculations, we did verify this formula though!

T_ν) into account as well. Nevertheless, given that energy transfer to the dark sector occurs primarily following neutrino kinetic decoupling, meaning $dS_\nu \simeq 0$ (where S_ν is the neutrino subsystem entropy), the net transfer of energy to the neutrino subsystem can be safely neglected. That said, we will still have to consider the evolution of T_ν, which nonetheless trivially scales as the inverse of the scale factor (see e.g. [58]).

We now proceed to express the 2nd law of thermodynamics. The variations in entropy in the visible $[dS]$ and dark $[dS']$ sectors are given by:

$$dS = -\frac{dQ}{T_\gamma} \;\; ; \;\; dS' = \frac{dQ}{T_{\gamma_D}} \; . \tag{2.7}$$

The entropy for a particle species with energy density ρ, pressure p and temperature T is (see for instance [58]):

$$S = \frac{\rho + p}{T} R^3 \; . \tag{2.8}$$

Taking the derivative with respect to time in Eqs.(2.7) and combining the result with Eqs.(2.4,2.8), after neglecting the neutrino contribution to the variation in entropy (which is warranted since $dS_\nu \simeq 0$), yields:[9]

$$\frac{d}{dt}\left[\frac{(\rho_\gamma + p_\gamma + \rho_e + p_e)R^3}{T_\gamma}\right] = -\frac{n_e n_{\bar{e}}\langle \sigma v_{M\o l}\mathcal{E}\rangle R^3}{T_\gamma} \; ,$$
$$\frac{d}{dt}\left[\frac{(\rho_{\gamma_D} + p_{\gamma_D} + \rho_{F_1} + p_{F_1})R^3}{T_{\gamma_D}}\right] = \frac{n_e n_{\bar{e}}\langle \sigma v_{M\o l}\mathcal{E}\rangle R^3}{T_{\gamma_D}} \; . \tag{2.9}$$

To describe the evolution of the scale factor, we make use of the Einstein field equations, which relate the geometry of the Universe to its energy content. The 00 component of the Einstein field equations, which is known as first Friedmann equation, reads:[10]

$$\left(\frac{\dot{R}}{R}\right)^2 = \frac{8\pi G_N}{3}\left[\rho_\gamma + \rho_e + \rho_\nu + \rho_{\gamma_D} + \rho_{F_1}\right] \; . \tag{2.10}$$

Denoting $x \equiv m_e/T_\gamma$, we can express energy densities and pressures for particle species in the visible sector as (see e.g. [58]):

$$\rho_\gamma = \frac{\pi^2}{15}T_\gamma^4 \; , \;\; \rho_e = \frac{2T_\gamma^4}{\pi^2}\int_x^\infty du \, \frac{(u^2 - x^2)^{\frac{1}{2}}u^2}{1 + e^u} \; , \;\; \rho_\nu = \frac{7\pi^2}{40}T_\nu^4 \; ,$$
$$p_\gamma = \frac{\pi^2}{45}T_\gamma^4 \; , \;\; p_e = \frac{2T_\gamma^4}{3\pi^2}\int_x^\infty du \, \frac{(u^2 - x^2)^{\frac{3}{2}}}{1 + e^u} \; . \tag{2.11}$$

Similarly, for particle species in the dark sector, with $x' \equiv m_{F_1}/T_{\gamma_D}$, we obtain:

$$\rho_{\gamma_D} = \frac{\pi^2}{15}T_{\gamma_D}^4 \; , \;\; \rho_{F_1} = \frac{2T_{\gamma_D}^4}{\pi^2}\int_{x'}^\infty du \, \frac{(u^2 - x'^2)^{\frac{1}{2}}u^2}{1 + e^u} \; ,$$
$$p_{\gamma_D} = \frac{\pi^2}{45}T_{\gamma_D}^4 \; , \;\; p_{F_1} = \frac{2T_{\gamma_D}^4}{3\pi^2}\int_{x'}^\infty du \, \frac{(u^2 - x'^2)^{\frac{3}{2}}}{1 + e^u} \; . \tag{2.12}$$

---

[9]For notational convenience, in Eqs.(2.9) and following, we have defined $\rho_e \equiv \rho_e + \rho_{\bar{e}}$, and similarly for p_e, ρ_{F_1} and p_{F_1}.

[10]The dot denotes a derivative with respect to time.

As we previously remarked, the neutrino temperature scales as $T_\nu \propto 1/R$, which can be obtained straightforwardly from $dS_\nu \simeq 0$. Since both sides of Eqs.(2.9) display the same power of the scale factor R and hence all proportionality factors cancel (rather conveniently!), we can effectively replace R in Eqs.(2.9) by $1/T_\nu$, and therefore express Eqs.(2.9) as:

$$\frac{d}{dt}\left[\frac{(\rho_\gamma + p_\gamma + \rho_e + p_e)}{T_\gamma T_\nu^3}\right] = -\frac{n_e n_{\bar{e}}\langle \sigma v_{M\o l}\mathcal{E}\rangle}{T_\gamma T_\nu^3} \, ,$$

$$\frac{d}{dt}\left[\frac{(\rho_{\gamma_D} + p_{\gamma_D} + \rho_{F_1} + p_{F_1})}{T_{\gamma_D} T_\nu^3}\right] = \frac{n_e n_{\bar{e}}\langle \sigma v_{M\o l}\mathcal{E}\rangle}{T_{\gamma_D} T_\nu^3} \, , \qquad (2.13)$$

and Eq.(2.10) as:

$$\frac{1}{T_\nu}\frac{dT_\nu}{dt} = -\sqrt{\frac{8\pi G_N}{3}\left(\rho_\gamma + \rho_e + \rho_\nu + \rho_{\gamma_D} + \rho_{F_1}\right)} \, . \qquad (2.14)$$

What we have just written down [Eqs.(2.13,2.14)] is a system of three differential equations for three unknowns: T_γ, T_{γ_D} and T_ν. If we provide initial conditions we can trace the evolution of these three quantities. Recall that our goal is to study the evolution of the quantity $X \equiv T_{\gamma_D}/T_\gamma$, subject to initial condition $X \simeq 0$. With some manipulation we can bring Eqs.(2.13) to the form:

$$\zeta\frac{dT_\gamma}{dt} + \kappa\frac{dT_\nu}{dt} = -\frac{n_e n_{\bar{e}}\langle \sigma v_{M\o l}\mathcal{E}\rangle}{T_\gamma^3} \; ; \; \zeta'\frac{dT_{\gamma_D}}{dt} + \kappa'\frac{dT_\nu}{dt} = \frac{n_e n_{\bar{e}}\langle \sigma v_{M\o l}\mathcal{E}\rangle}{T_{\gamma_D}^3} \, , \qquad (2.15)$$

where we have defined:

$$\zeta \equiv \frac{3\rho_\gamma}{T_\gamma^4} + \frac{3p_\gamma}{T_\gamma^4} + \frac{3\rho_e}{T_\gamma^4} + \frac{3p_e}{T_\gamma^4} + \frac{2m_e^2}{\pi^2 T_\gamma^2}\int_x^\infty du\, \frac{(u^2 - x^2)^{-\frac{1}{2}}u^2 + (u^2 - x^2)^{\frac{1}{2}}}{1 + e^u} \, ,$$

$$\zeta' \equiv \frac{3\rho_{\gamma_D}}{T_{\gamma_D}{}^4} + \frac{3p_{\gamma_D}}{T_{\gamma_D}{}^4} + \frac{3\rho_{F_1}}{T_{\gamma_D}{}^4} + \frac{3p_{F_1}}{T_{\gamma_D}{}^4} + \frac{2m_{F_1}^2}{\pi^2 T_{\gamma_D}{}^2}\int_{x'}^\infty du\, \frac{(u^2 - x'^2)^{-\frac{1}{2}}u^2 + (u^2 - x'^2)^{\frac{1}{2}}}{1 + e^u} \, ,$$

$$\kappa \equiv -\left(\frac{3\rho_\gamma}{T_\gamma^3} + \frac{3p_\gamma}{T_\gamma^3} + \frac{3\rho_e}{T_\gamma^3} + \frac{3p_e}{T_\gamma^3}\right)\frac{1}{T_\nu} \, , \quad \kappa' \equiv -\left(\frac{3\rho_{\gamma_D}}{T_{\gamma_D}{}^3} + \frac{3p_{\gamma_D}}{T_{\gamma_D}{}^3} + \frac{3\rho_{F_1}}{T_{\gamma_D}{}^3} + \frac{3p_{F_1}}{T_{\gamma_D}{}^3}\right)\frac{1}{T_\nu} \, . \quad (2.16)$$

The system given by Eqs.(2.14,2.15) can now be solved numerically.[11] An example of such a solution is presented in Figure 2.2, where we plot the evolution of T_{γ_D}/T_γ as a function of T_γ for different values of m_{F_1} and for $\epsilon = 10^{-9}$. Note that time flows from the right to the left.

The reader can infer from Figure 2.2 that at late times T_{γ_D}/T_γ asymptotically approaches a constant, for which we would like to find an approximate analytic expression. But before doing so it is convenient to remind ourselves of the results obtained in the MDM framework, which can be seen as a special case of our model where $m_{F_1} = m_e$, with the main process governing energy transfer between the sectors being $e\bar{e} \to e'\bar{e}'$. In [34] it was determined that, in the limit $T_\gamma \gg m_e$, the ratio $T_{\gamma'}/T_\gamma$ (γ' being the mirror photon, analogous, of course, to our dark photon), subject to initial condition $T_{\gamma'} = 0$ at $T_\gamma = T_i$, evolved according to:

$$\frac{T_{\gamma'}}{T_\gamma} \propto \sqrt{\epsilon}\left[\frac{1}{T_\gamma} - \frac{1}{T_i}\right]^{\frac{1}{4}} \, . \qquad (2.17)$$

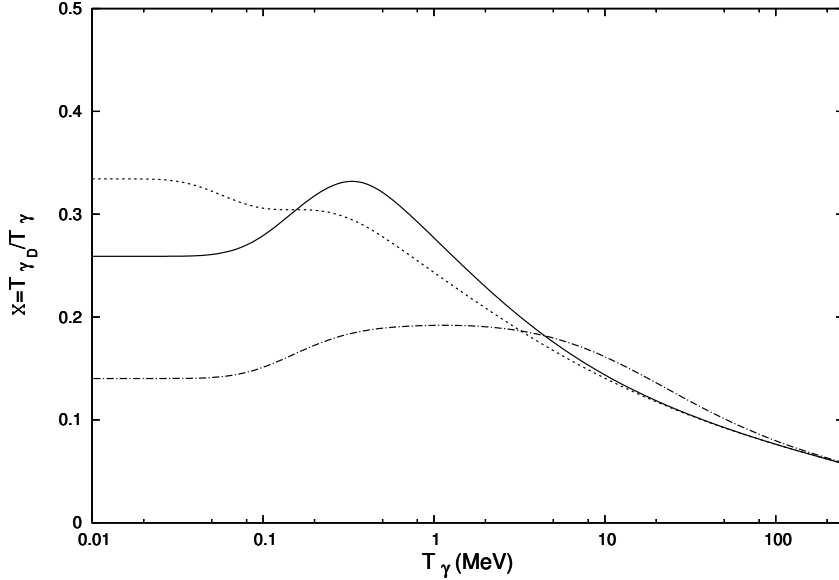[11]We employed a straightforward numerical integration routine in FORTRAN77.

Figure 2.2: Evolution of $X \equiv T_{\gamma_D}/T_\gamma$ for $m_{F_1} = 10$ MeV (dot-dashed line), $m_{F_1} = 1$ MeV (solid line) and $m_{F_1} = 0.1$ MeV (dashed line).

For temperatures below m_e, Boltzmann suppression of e and $\bar{e}$ number densities means that energy transfer to the mirror sector is halted, given that the rate for the relevant process drops exponentially.

The result obtained for MDM can easily be generalized to the case we are analysing. The rate for the relevant process here, $e\bar{e} \to F_1\bar{F}_1$, drops significantly when the temperature reaches $T_\gamma \sim \mathcal{M} \equiv \max(m_e, m_{F_1})$ which, jointly with Eq.(2.17), suggests that the asymptotic value of X is proportional to $\sqrt{\epsilon}(m_e/\mathcal{M})^{\frac{1}{4}}$. We corroborated this result numerically, by studying the evolution of X for varying values of ϵ and m_{F_1}, finding that the asymptotic value of the ratio of the temperature in the two sectors, T_{γ_D}/T_γ, for parameters in the range $10^{-10} \lesssim \epsilon \lesssim 10^{-7}$ and 0.1 MeV $\lesssim m_{F_1} \lesssim$ 100 MeV, can be expressed as[12]:

$$\frac{T_{\gamma_D}}{T_\gamma} \simeq 0.31 \sqrt{\frac{\epsilon}{10^{-9}}} \left(\frac{m_e}{\mathcal{M}}\right)^{\frac{1}{4}} , \quad \mathcal{M} \equiv \max(m_e, m_{F_1}) . \tag{2.18}$$

The shape of the curves in Figure 2.2 can be easily explained. At early times, that is, for $T_\gamma \gg \mathcal{M}$, the curves ascend following a $(1/T_\gamma)^{\frac{1}{4}}$ behavior, consistent with our analytical considerations. A deviation from the analytic solution occurs for $T_\gamma \sim \mathcal{M}$. After then, the characteristic bumps displayed by the curves can be brought back to annihilation processes (e-$\bar{e}$ and F_1-$\bar{F}_1$ annihilations) which heat the respective sectors at approximately the temperature corresponding to the mass of the particle pair that annihilates. Once these annihilations are over, X reaches its asymptotic value, for which we found an analytic estimate [Eq.(2.18)].

2.2 Constraints from additional energy density

Where to from here? As affirmed initially, early Universe cosmology (and in particular BBN and LSS formation), as currently understood, places strong constraints on exotic contributions to the energy density during the radiation dominated era. In particular, the relativistic

---

[12]Unsurprisingly, we have recovered the same numerical factor as in MDM, where it has been found that $T_{\gamma'}/T_\gamma$ asymptotically evolves to $0.31\sqrt{\epsilon/10^{-9}}$ [35].

energy density component is subject to tight bounds, which we here wish to exploit. Fortunately for us, there is a relatively simple and useful way of parametrizing the relativistic energy density component, that is, via an effective number of neutrino species. We have fairly robust constraints on this quantity arising from cosmological observations. In the following we consider the effects of extra energy density at the epoch of Hydrogen recombination first and BBN afterwards, parametrizing it in terms of an effective number of neutrino species, which we then use to set constraints on the available parameter space.

2.2.1 Calculation of $\delta N_{\text{eff}}[\text{CMB}]$

We begin by computing the additional contributions to the relativistic energy density at Hydrogen recombination. The relativistic energy density at this epoch can be expressed as:

$$\rho_{\text{rad}} = \left(1 + \frac{7}{8}\left(\frac{4}{11}\right)^{\frac{4}{3}} N_{\text{eff}}[\text{CMB}]\right)\rho_\gamma \, , \tag{2.19}$$

where the factor of 4/11 accounts for γ heating by e-$\bar{e}$ annihilation, following neutrino kinetic decoupling, and the factor of 7/8 owes its presence to the different statistical nature (fermionic instead of bosonic) of neutrinos with respect to photons (see [58] for more in-depth discussions). But the quantity we really are interested in here is N_{eff}, known as the effective number of neutrino species. The SM, as is well known, makes the prediction $N_{\text{eff}} = 3.046$. Exotic contributions to the relativistic energy density at Hydrogen recombination are then encoded via $\delta N_{\text{eff}}[\text{CMB}] \equiv N_{\text{eff}}[\text{CMB}] - 3.046$, which is constrained by several observations, for instance that from WMAP [5], the Atacama Cosmology Telescope [60], the South Pole Telescope [61] and the recent results from the Planck mission [9]. The observations are consistent with the SM predictions and to an approximate 2σ limit provide the constraint $\delta N_{\text{eff}}[\text{CMB}] < 0.84$ [9]. Note that $\delta N_{\text{eff}}[\text{CMB}]$ can be conveniently expressed as:

$$\delta N_{\text{eff}}[\text{CMB}] = 3\left(\left[\frac{T_\nu(\epsilon)}{T_\nu(\epsilon = 0)}\right]^4 - 1\right) + \frac{8}{7}\left(\frac{T_{\gamma_D}(\epsilon)}{T_\nu(\epsilon = 0)}\right)^4 \, , \tag{2.20}$$

where all temperatures are evaluated at photon decoupling, $T_\gamma \simeq 0.26$ eV. Two effects contribute to increasing $N_{\text{eff}}[\text{CMB}]$, and are accounted for by the two terms in Eq.(2.20): the first is the increase of T_{γ_D} at the expense of T_γ, which reduces T_γ/T_ν and has the net effect of increasing the number of neutrino species at Hydrogen recombination; the second is obviously the increase in N_{eff} due to an increase in T_{γ_D} itself.

Making use of Eqs.(2.14,2.15,2.20), we evaluate $\delta N_{\text{eff}}[\text{CMB}]$ for some example parameter choice, before proceeding to constrain the available parameter space by imposing the condition $\delta N_{\text{eff}}[\text{CMB}] < 0.84$. We anticipate that the addition of extra energy density, parametrized by $\delta N_{\text{eff}}[\text{CMB}]$, is not the only effect we have to consider for the CMB. Another, and for that matter more important, piece of new physics to consider is that of dark acoustic oscillations, which we will deal with in Chapter 2.3. In Figure 2.3 we plot $\delta N_{\text{eff}}[\text{CMB}]$ against ϵ keeping m_{F_1} fixed. We find that the bounds on ϵ arising from constraints on $\delta N_{\text{eff}}[\text{CMB}]$ (which will be presented in Figure 2.4) can be expressed as:

$$\epsilon \lesssim 3.5 \times 10^{-9} \left(\frac{\mathcal{M}}{m_e}\right)^{\frac{1}{2}} \, . \tag{2.21}$$

The $\epsilon \propto \mathcal{M}^{\frac{1}{2}}$ dependence can be readily understood by referring to Eqs.(2.18,2.20). Note also that, for $\mathcal{M} = m_e$, we have recovered the numerical factor of 3.5×10^{-9} obtained in analogous studies in the MDM framework [30, 35].
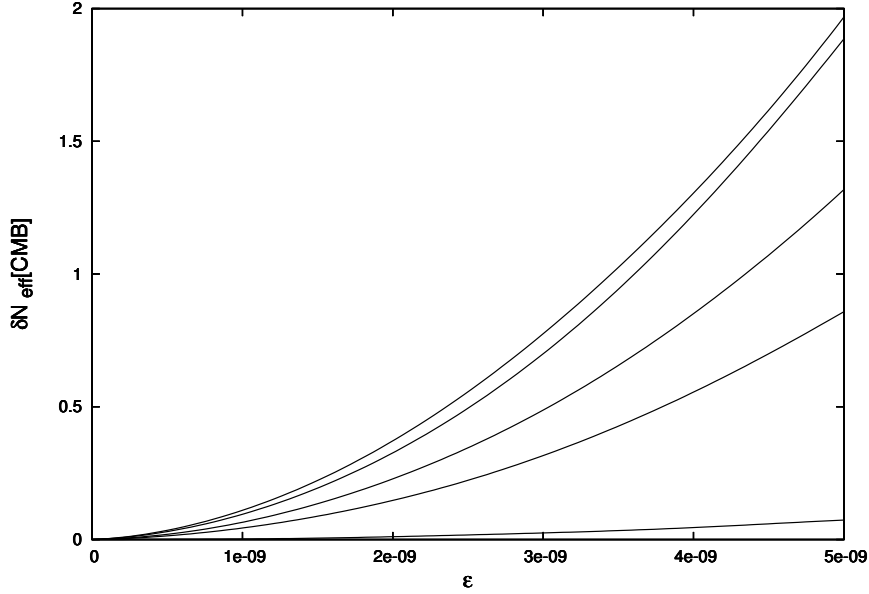
Figure 2.3: $\delta N_{\text{eff}}[\text{CMB}]$ versus ϵ for fixed m_{F_1} values; going from up to down, $m_{F_1} = 0.1, 0.5, 0.7, 1, 10$ MeV.

2.2.2 Calculation of $\delta N_{\text{eff}}[\text{BBN}]$

We now inquire as to how the addition of energy density during the early Universe affects BBN. Recall that BBN is the process during which light nuclei, notably Helium, were synthesized (refer to Steven Weinberg's book [62] for an in-depth review on the topic) It is well known that an increase in the energy density by the addition of one neutrino species has the effect of increasing the Helium fraction, Y_p, by approximately 0.013 [63]. *Ergo*, the change in neutrino species associated with BBN can be identified with:

$$\delta N_{\text{eff}}[\text{BBN}] = \frac{Y_p(\epsilon) - Y_p(\epsilon = 0)}{0.013} . \tag{2.22}$$

The synthesis of Helium proceeds via that of deuterium. This, in turn, depends on the neutron abundance, $X_n \equiv n_p/(n_n + n_p)$, where $n_n[n_p]$ stands for the neutron [proton] number density. The neutron abundance is affected by the following weak interaction processes:

$$n + \nu_e \leftrightarrow p + e \, , \, n + \bar{e} \leftrightarrow p + \bar{\nu}_e \, , \, n \rightarrow p + e + \bar{\nu}_e \, . \tag{2.23}$$

Initially, at equilibrium (that is, for $T_\gamma \gg m_n$), $X_n \simeq (1 + e^{Q/T})^{-1}$, where $Q = m_n - m_p \simeq 1.293\,\text{MeV}$ is the mass difference between the neutron and the proton.

The four processes which affect X_n (excluding neutron decay) proceed at the following rates, which can be found in e.g. [62]:

$$\lambda_1 \equiv \lambda(n + \nu_e \rightarrow p + e) = \mathcal{B} \int_0^\infty dP_\nu \, E_e^2 P_\nu^2 \frac{1}{e^{\frac{E_\nu}{T_\nu}} + 1} \frac{1}{e^{-\frac{E_e}{T_\gamma}} + 1} \, , \tag{2.24}$$

$$\lambda_2 \equiv \lambda(n + \bar{e} \rightarrow p + \bar{\nu}_e) = \mathcal{B} \int_0^\infty dP_e \, E_\nu^2 P_e^2 \frac{1}{e^{\frac{E_e}{T_\gamma}} + 1} \frac{1}{e^{-\frac{E_\nu}{T_\nu}} + 1} \, , \tag{2.25}$$

$$\lambda_3 \equiv \lambda(p + e \rightarrow n + \nu_e) = \mathcal{B} \int_{\sqrt{Q^2 - m_e^2}}^\infty dP_e \, E_\nu^2 P_e^2 \frac{1}{e^{\frac{E_e}{T_\gamma}} + 1} \frac{1}{e^{-\frac{E_\nu}{T_\nu}} + 1} \, , \tag{2.26}$$

$$\lambda_4 \equiv \lambda(p + \bar{\nu}_e \rightarrow n + \bar{e}) = \mathcal{B} \int_{Q + m_e}^\infty dP_\nu \, E_e^2 P_\nu^2 \frac{1}{e^{\frac{E_\nu}{T_\nu}} + 1} \frac{1}{e^{-\frac{E_e}{T_\gamma}} + 1} \, . \tag{2.27}$$

In the above we have indicated by $E_e[E_v]$, $P_e[P_v]$ the electron [neutrino] energy and momentum respectively, and have obtained the extremals of the integrals from straightforward kinematical considerations. The other factors within the integrals take into account the effects of Fermi-Dirac statistics and Pauli blocking; the constant $\mathcal{B}$ is given by $\mathcal{B} = G_F^2(1 + 3g_A^2)\cos^2\theta_c/(2\pi^3)$, where $G_F = 1.166 \times 10^{-5}$ GeV^{-2}, $g_A = 1.257$ and $\cos\theta_c = 0.97456$. Defining $\lambda_n^{-1} = \tau_n \simeq 886.7$ s to be the neutron lifetime, the evolution of the neutron fraction is governed by the following differential equation:

$$\frac{dX_n}{dt} = -(\lambda_1 + \lambda_2 + \lambda_n)X_n + (\lambda_3 + \lambda_4)(1 - X_n) . \tag{2.28}$$

We evolve the neutron fraction down to the *deuterium bottleneck temperature* (DBT), $T_\gamma \simeq 0.07$ MeV (see e.g. [6]), by solving Eq.(2.28) simultaneously with Eqs.(2.14,2.15); the latter two are employed to obtain the modified time-temperature relation. The helium fraction, Y_p, is twice the value of the neutron fraction at the DBT, and we can thus evaluate $\delta N_{\text{eff}}[\text{BBN}]$ via Eq.(2.22). At around 95% confidence level, the data constrains $\delta N_{\text{eff}}[\text{BBN}] < 1$ [64], which we make use of to set bounds on the available parameter space. In Figure 2.4 we display the constraints which follow from this analysis together with those set from $\delta N_{\text{eff}}[\text{CMB}]$ considerations. As is visually clear, the bounds deriving from $\delta N_{\text{eff}}[\text{CMB}]$ are more stringent than those arising from $\delta N_{\text{eff}}[\text{BBN}]$.
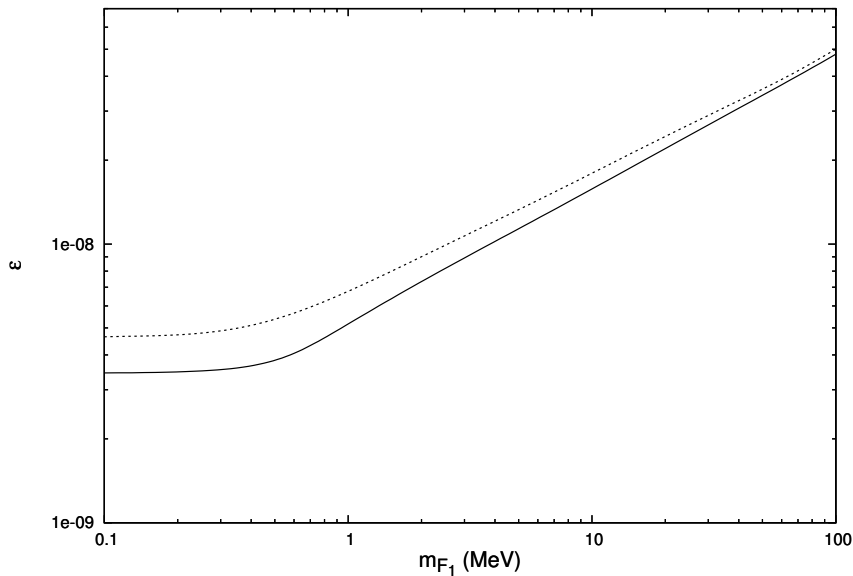
Figure 2.4: Exclusion limits derived from the requirements $\delta N_{\text{eff}}[\text{CMB}] < 0.84$ (above solid line) and $\delta N_{\text{eff}}[\text{BBN}] < 1$ (above dashed line) in ϵ-m_{F_1} parameter space.

2.3 Dark recombination

In an endeavor to set constraints on our dark matter model, we have probed a piece of new physics which affects the CMB. That is, the additional energy density at Hydrogen recombination, as parametrized by $\delta N_{\text{eff}}[\text{CMB}]$. Still, another and yet more momentous bit of new physics affecting the CMB is represented by dark acoustic oscillations. As the temperature of the Universe drops, it becomes increasingly energetically unfavourable for dark matter to remain ionized. Eventually, F_1 and F_2 will combine into neutral dark states, in a process known as *dark recombination*. Prior to dark recombination, though, dark matter

behaves as a tightly coupled fluid which undergoes dark acoustic oscillations. This should not come as a surprise, given that an analogous phenomenon takes place in the visible sector prior to Hydrogen recombination. Clearly, these oscillations suppress power on small scales, and hence represent a noteworthy deviation from collisionless CDM. Eventually, such a suppression of power on small scales might provide aid in addressing the missing satellite problem, that is, the observed shortage of dwarf galaxies in the neighborhood of the Milky Way [13].

Nevertheless, successful LSS formation sets sturdy constraints on the physics of dark acoustic oscillations. As long as dark matter remains ionized, interactions with dark photons will wash out dark matter overdensities which, the reader will recall, provide the potential wells within which the photon-baryon fluid oscillates. Given that overdensities driven by gravitational attraction can only begin to grow substantially following matter-radiation equality, it is important to require that dark recombination occurs before then. Delaying the onset of structure formation would result in LSS formation which is inconsistent with observations. Hence, in this work we derive bounds on our model by requiring $T_{dr} \gtrsim T_{eq}$, where T_{dr} and T_{eq} denote the temperatures in the visible sector at the time of dark recombination and matter-radiation equality respectively. This condition has been used in the literature (see for instance [65], which followed from other works in the MDM framework, e.g. [33, 66, 67]) and ensures that dark acoustic oscillations do not tamper with the early growth of LSS.

2.3.1   Saha equation

In the dark matter model under inspection, dark recombination consists of the process during which $|Z'| F_1$ particles combine with one F_2 particle to form a neutral dark state, which we call D^0. The crucial moment, that is, the transition from ionized to neutral dark matter, occurs when the last F_1 particle combines with the dark state consisting of $(|Z'| - 1) F_1$ particles and one F_2 particle. Following the convention where F_1 has charge -1 and F_2 has charge $|Z'|$, it is natural to denominate this state D^+, and hence the process we wish to examine is:

$$F_1 + D^+ \leftrightarrow D^0 + \gamma_D . \tag{2.29}$$

In order to inspect the process in Eq.(2.29) and determine when dark recombination occurs, we trace the abundances of the species in question. A handy way of doing so is by writing down the relevant Saha equation, which is given by (see e.g. [6]):

$$\frac{n_{D^0}}{n_{D^+} n_{F_1}} = \frac{n_{D^0}^{(0)}}{n_{D^+}^{(0)} n_{F_1}^{(0)}} , \tag{2.30}$$

with the superscript $^{(0)}$ denoting an equilibrium value. The reader should be wary of the fact that Eq.(2.30) arises as the equilibrium limit of the Boltzmann equations. As a consequence, the Saha equation does not follow the abundances of particle species correctly through non-equilibrium processes, for instance freeze-out. Nevertheless, it does a good job in establishing the redshift of dark recombination, which is the quantity we are interested in determining [6].

As it turns out, it is actually more befitting to express Eq.(2.30) in a different form, by tracing the ionization fraction of F_1, rather than its number density; *ergo*, we introduce the ionization fraction of F_1, χ:

$$\chi \equiv \frac{n_{F_1}}{n_{F_2}} = \frac{n_{F_1}}{n_{F_1} + n_{D^0}} = \frac{n_{F_1}}{n_{D^+} + n_{D^0}} , \tag{2.31}$$

where n_{F_1} is the number density of free F_1 particles and n_{F_2} is the total number density of F_2 particles. The last equality follows from assuming $U(1)'$ neutrality. Correspondingly, the left-hand side of Eq.(2.30) is simply $(1 - \chi)/n_{F_2}\chi^2$. The right-hand side of Eq.(2.30) can also be manipulated into a more useful form. Consider a particle species P of mass m_P and temperature T_P. Its equilibrium number density, in the limit where $m_P \gg T_P$, can be expressed as (see e.g. [6]):

$$n_P = g_P \left(\frac{m_P T_P}{2\pi} \right)^{\frac{3}{2}} e^{-\frac{m_P - \mu_P}{T_P}} , \tag{2.32}$$

where μ_P denotes the chemical potential and g_P is a degeneracy factor which customarily accounts for multiple spin states. Given that $\mu_{\gamma_D} = 0$ to good approximation then, as long as equilibrium holds, $\mu_{F_1} + \mu_{D^+} = \mu_{D^0}$ applies. Additionally, we define the ionization energy of D^0 to be $I' = m_{F_1} + m_{D^+} - m_{D^0}$. Under the approximation $m_{D^+} \simeq m_{D^0}$ (which follows from $m_{F_2} \gg m_{F_1}$) and making use of the fact that $g_{F_1} g_{D^+} = g_{D^0}$, we can rearrange the right-hand side of Eq.(2.30) to being $(2\pi/m_{F_1} T_{\gamma_D})^{3/2} e^{I'/T_{\gamma_D}}$, and hence express Eq.(2.30) as follows:

$$\frac{1 - \chi}{\chi^2} = n_{F_2} \left(\frac{2\pi}{m_{F_1} T_{\gamma_D}} \right)^{\frac{3}{2}} e^{\frac{I'}{T_{\gamma_D}}} . \tag{2.33}$$

To make progress, we have to provide an expression for the F_2 number density. We note that it simply scales as the number density of baryons in the visible sector, n_b:

$$n_{F_2} = \left(\frac{\Omega_{\rm dm}}{\Omega_b} \right) \left(\frac{m_p}{m_{F_2}} \right) n_b = \left(\frac{\Omega_{\rm dm}}{\Omega_b} \right) \left(\frac{m_p}{m_{F_2}} \right) \left(\frac{n_b}{n_\gamma} \right) \left(\frac{n_\gamma}{n_{\gamma_D}} \right) n_{\gamma_D} . \tag{2.34}$$

In the above $m_p \simeq 0.94$ GeV is the proton mass and $\eta \equiv n_b/n_\gamma$ is the baryon-to-photon ratio. By using $\Omega_{\rm dm}/\Omega_b \simeq 5.4$ [9], $\eta \simeq 6 \times 10^{-10}$ [68], $n_\gamma/n_{\gamma_D} = \left(T_\gamma/T_{\gamma_D} \right)^3$ [with T_γ/T_{γ_D} evaluated using Eq.(2.18)] and $n_{\gamma_D} = \pi^2 T_{\gamma_D}^3/45$, Eq.(2.33) can be put to the form:

$$\frac{1 - \chi}{\chi^2} = \mathcal{A} \left(\frac{T_{\gamma_D}}{I'} \right)^{\frac{3}{2}} e^{\frac{I'}{T_{\gamma_D}}} , \tag{2.35}$$

where we have defined:

$$\mathcal{A} \simeq 3.5 \times 10^{-7} \left(\frac{10^{-9}}{\epsilon} \right)^{\frac{3}{2}} \left(\frac{\mathcal{M}}{m_e} \right)^{\frac{3}{4}} \left(\frac{\rm GeV}{m_{F_2}} \right) \left(\frac{I'}{m_{F_1}} \right)^{\frac{3}{2}} . \tag{2.36}$$

The final step is to switch to the variable $\xi \equiv I'/T_{\gamma_D}$, so that Eq.(2.35) becomes:

$$\frac{1 - \chi}{\chi^2} = \mathcal{A} \xi^{-\frac{3}{2}} e^\xi . \tag{2.37}$$

We can solve Eq.(2.37) to determine the redshift of dark recombination, which takes place when the ionization fraction of F_1 is approximately 10%, i.e. for $\chi \simeq 0.1$. Substituting $\chi = 0.1$ into Eq.(2.37), it follows that the equation we have to solve is:

$$\xi = \frac{3}{2} \ln \xi + \ln \left(\frac{90}{\mathcal{A}} \right) . \tag{2.38}$$

It is straightforward to solve Eq.(2.38) numerically (for example by iteration). The temperature of the visible sector at dark recombination, $T_{\rm dr}$, is found by inverting Eq.(2.18), with $T'_{\rm dr} = I'/\xi$, where ξ solves Eq.(2.38):

$$T_{\rm dr} \simeq 3.2 \left(\frac{10^{-9}}{\epsilon} \right)^{\frac{1}{2}} \left(\frac{\mathcal{M}}{m_e} \right)^{\frac{1}{4}} \frac{I'}{\xi} . \tag{2.39}$$

2.3.2 Binding energy of the dark bound state

We are not quite there yet, for the value of the constant $\mathcal{A}$ in Eq.(2.36) contains I', the ionization energy of the dark bound state, which is *a priori* unknown. We note that our bound system of one F_2 particle with N F_1 particles is analogous to that of ordinary nuclei with N electrons. It then follows that the binding energy of D^0 assumes the general form:

$$I' = Z'^2_{\text{eff}} \frac{\alpha'^2}{2} \mu_R \,, \tag{2.40}$$

where $\mu_R = m_{F_1} m_{D^+}/(m_{F_1} + m_{D^+})$ is the reduced mass of the F_1-D^+ system. In the limit where $m_{F_2} \gg m_{F_1}$, we obtain that $I' \simeq Z'^2_{\text{eff}} \alpha'^2 m_{F_1}/2$. Therefore, the problem of determining I' (and hence being able to solve the Saha equation) has been reduced to the problem of determining Z'_{eff}. Alas, this is by no means a simple issue, as Z'_{eff} depends on the shielding caused by the $(|Z'|-1)$ F_1 particles, which partially conceal the charge of the F_2 particle. Understanding the exact details of this shielding mechanism would require solving a complicated many-body problem! Nevertheless, let us remark that the exact same phenomenon occurs in ordinary nuclei with atomic number Z, where $(Z-1)$ electrons shield the nucleus from the last electron. Even though exact analytic expressions for Z'_{eff} are generally unknown, we note that it only depends on the chemistry of the bound state, that is, on the arrangement of F_1 particles in orbitals.

The above realisation justifies the claim that I' is related to I, the binding energy of the corresponding ordinary element with atomic number $Z = Z'$, by a simple scaling relation:

$$I' = \left(\frac{\alpha'}{\alpha}\right)^2 \left(\frac{m_{F_1}}{m_e}\right) I \,. \tag{2.41}$$

In Figure 2.5 we plot the binding energies of the elements of the periodic table as a function of the atomic number Z. We see that, apart from isolated cases such as Helium and Neon and, more generally, excluding noble gases, the binding energies of the various elements reside in a fairly narrow range centered at about 10 eV, to within a factor of uncertainty of approximately 2. For $Z \gtrsim 10$, the dependence of I on Z is weaker still. In other words, $Z'_{\text{eff}} \approx 1$ (and hence $I' \approx \alpha'^2 m_{F_1}/2$) in Eq.(2.40), which should not come as a surprise given that, to first rough approximation, the dark charge seen by the last F_1 particle is approximately 1.
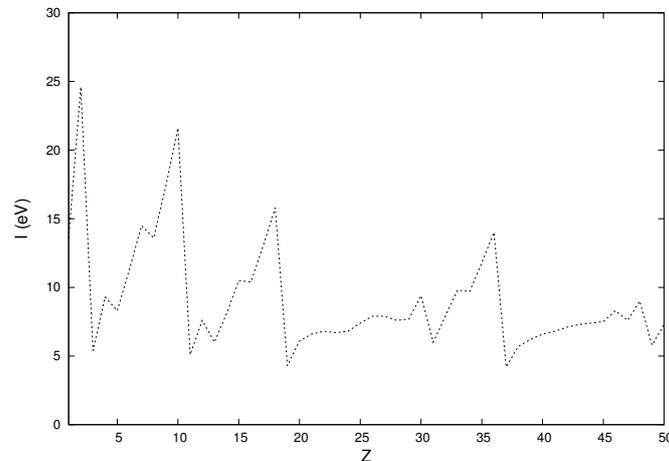

Figure 2.5: Ionization energy as a function of atomic number for ordinary elements.

2.3.3 Exclusion limits

Having devised a way of obtaining the binding energy of D^0, we now proceed to place bounds on the parameter space of our model. Recall we do so by requiring $T_{dr} \gtrsim T_{eq}$, where T_{eq} is the temperature of the visible sector at matter-radiation equality, which occurs at a redshift $z_{eq} = 3200 \pm 130$ [68]. This leads to a lower limit on the matter-radiation equality temperature of $T_{eq} \simeq 0.72$ eV.

In principle we would have to examine a 5-dimensional parameter space, spanned by $m_{F_1}, m_{F_2}, \alpha', Z'$ and ϵ. Nevertheless, we claim that it will be sufficient to examine three of them to obtain a good understanding of the physics of dark recombination. In fact, a numerical analysis of our solution exhibits a weak dependence on m_{F_2}. This is not surprising, since one can easily check that an iterative solution of Eq.(2.38) presents a log-like dependence on the value of the constant $\mathcal{A}$, which is the only place where the mass of the F_2 particle appears. Moreover, as we have discussed in the previous section, the dependence on Z' is also reasonably minor, given that it affects the binding energy in a limited way. These considerations appear to justify, to reasonable approximation, our claim that the physics of dark recombination is dictated solely by three parameters: m_{F_1}, α' and ϵ. We now proceed to examine the relevant 3-dimensional parameter space.

Recall we began by solving the Saha equation to obtain T_{dr}, following which we imposed $T_{dr} \gtrsim T_{eq}$. From Eq.(2.41) we see that $T'_{dr} \propto I' \propto \alpha'^2 m_{F_1}$. Employing Eq.(2.18) it then follows that $T_{dr} = T'_{dr}(T_{dr}/T'_{dr}) \propto \alpha'^2 m_{F_1} \mathcal{M}^{\frac{1}{4}}/\sqrt{\epsilon}$, and hence the upper limit on ϵ scales as $\alpha'^4 m_{F_1}^2 \sqrt{\mathcal{M}}$. The analytical analysis just presented is indeed confirmed by our numerical results, which we present in Figure 2.6, where we display the upper bound on ϵ for a fixed m_{F_1} and varying α'.
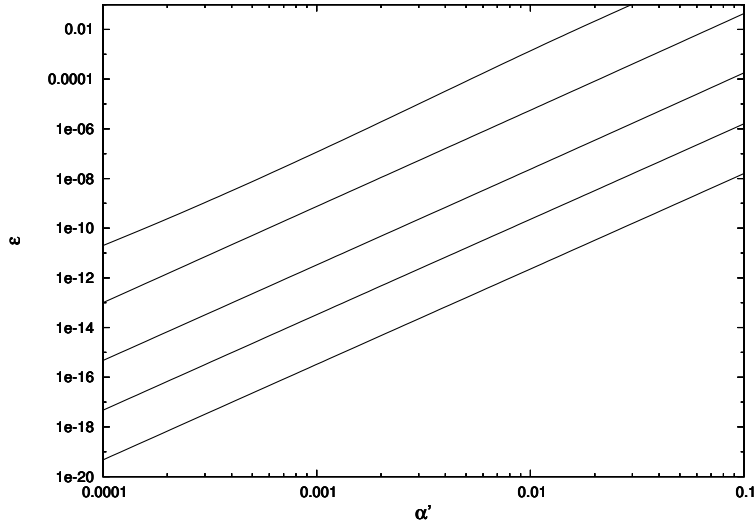
Figure 2.6: Exclusion limits from the constraint on the temperature of dark recombination (discussed in text). The limits are for fixed values of m_{F_1} for (going from upper to lower line) $m_{F_1} = 100, 10, 1, 0.1, 0.01$ MeV (excluded region is above the line).

In fine, we find that the upper bound on ϵ arising from the analysis of dark acoustic oscillations (subject to an uncertainty of a factor of approximately 2, which arises from having neglected the dependence on Z') can be expressed as:

$$\epsilon \lesssim 10^{-8} \left(\frac{\alpha'}{\alpha}\right)^4 \left(\frac{m_{F_1}}{\text{MeV}}\right)^2 \left(\frac{\mathcal{M}}{m_e}\right)^{\frac{1}{2}} , \tag{2.42}$$

where we remind the reader that $\mathcal{M} \equiv \max(m_e, m_{F_1})$.

THE STRUCTURE OF SPIRAL GALAXIES

3.1 Dynamical halo model and halo scaling relations

While a variety of hidden sector dark matter models have been studied in the context of early Universe cosmology, the vast and fascinating area of galaxy formation and structure remains to a great extent uncharted. Ultimately, a compelling dark matter model is required to explain a series of small scale structure observations, in a manner which is still to be determined. For instance, observations have inferred the presence of cores in the dark matter halos of spiral galaxies; furthermore, the product of the core densities and core radii appears to be approximately constant along their spectrum. Another puzzling observational feature of spiral galaxies is the Tully-Fisher relation, which correlates their luminosities and asymptotical rotational velocities. Collisionless CDM as currently understood appears unable to address these issues. It is possible (and likely) of course that our understanding of collisionless CDM is incomplete; for instance, a more thorough grasp of baryonic feedback processes and baryonic physics in general could provide aid in tackling these problems.

On the other hand, it is possible that a richer dark matter structure, comprising for instance self-interactions and dissipation, could be the key to explaining some of the observational properties listed above. In this Chapter, we delve into a study of spiral galaxies, in an attempt to verify whether our dissipative HS dark matter model is capable of explaining their structure and dynamics (and, to a lesser extent, that of irregular and elliptical galaxies). Not only will we find this to be possible, but we will demonstrate how it has the potential to unravel the origin of a series of unexplained properties of these galaxies (some of which have already been mentioned above). Before doing so, let us review some of the features of spiral galaxies.

Different components make up spiral galaxies. The main luminous one is a flat disk of baryonic matter, with spiral-shaped density enhancements in it, which give rise to the characteristic observed spiral pattern. These spirals are quasi-stationary traits, whose explanation involves density waves[1]. In some spiral galaxies, a spheroidal bulge resides in the middle of the disk. Within the bulge mostly old stars and globular clusters are present. The galactic center of spiral galaxies encompasses a supermassive black hole (SMBH) of mass $10^6 - 10^9 M_\odot$. The accretion of matter onto the SMBH results in a very strong emission in the radio and X-ray frequencies. In addition, the mass of the SMBH is correlated to the velocity dispersion of the stars in the bulge via what is known as the *M-σ relation*.

Finally, the entire baryonic disk is surrounded by a dark matter halo, which extends well beyond the visible regions of the galaxy, and is responsible for the inferred flat rotation curves. A simple application of Kepler's law allows us to establish that, far from the galactic center, the mass enclosed within a radius r increases linearly with r, and hence the density profile drops as $\rho \propto r^{-2}$. The nature, behaviour and dynamics of the dark matter halo in spiral (and, to a lesser extent, irregular and elliptical) galaxies will be our topic of discussion for the rest of the Chapter.

---

[1]This mechanism is quite analogous to that of a traffic jam, through which the motion of the slower moving cars leads to a density enhancement. Furthermore, the collective motion of the traffic jam is not related to the speed of the cars within it (see e.g. [69]).

Within the framework of our model, the dark matter halo consists of a plasma of F_1 and F_2 particles. The masslessness of the dark photon implies that energy can be lost to dissipative interactions between dark matter particles, such as thermal dark bremsstrahlung. The careful reader will then have realized that the model faces essentially the same problem as MDM does in this context, the radiative cooling problem. The dissipative interactions entail energy loss on a timescale which is significantly less than the Hubble time. The picture we have presented requires a sizeable heat source that can replace the energy lost. As in the MDM framework, we will argue that it is possible for ordinary supernovae to provide the halo with the required heat source: kinetic mixing induced processes are expected to convert a relevant fraction ($\lesssim 1/2$) of the core-collapse energy into F_1-$\bar{F}_1$ pairs and γ_Ds, ultimately reprocessed solely into dark photons. These dark photons can then heat the halo via a number of mechanisms, which we will discuss in more depth in the following pages. As we outlined in Chapter 2, this argument suggests that $m_{F_1} \lesssim 100$ MeV, else its pair production mechanism becomes Boltzmann suppressed.

The dynamics of the dark plasma are dictated by the Euler equations of fluid dynamics:

$$\frac{\partial \rho}{\partial t} + \nabla \cdot (\rho \mathbf{v}) = 0 \,,$$

$$\frac{\partial \mathbf{v}}{\partial t} + (\mathbf{v} \cdot \nabla)\mathbf{v} = -\left(\nabla \phi + \frac{\nabla P}{\rho} \right) \,,$$

$$\frac{\partial}{\partial t}\left[\rho \left(\frac{\mathbf{v}^2}{2} + \mathcal{E} \right) \right] + \nabla \cdot \left[\rho \left(\frac{\mathbf{v}^2}{2} + \frac{P}{\rho} + \mathcal{E} \right) \mathbf{v} \right] - \rho \mathbf{v} \cdot \nabla \phi = \frac{d\Gamma_{\text{heat}}}{dV} - \frac{d\Gamma_{\text{cool}}}{dV} \,. \tag{3.1}$$

In the above P, ρ, $\mathbf{v}$ and $\mathcal{E}$ denote the pressure, mass density, velocity and internal energy per unit mass of the fluid respectively. The heating and cooling rates are given by Γ_{heat} and Γ_{cool}. The above equations are notoriously hard to solve! If we wish to get some analytical insight from them, we will have to make some simplifying assumptions, together with having an eye for symmetry. Let us assume, to begin with, that the system evolves to a static configuration (whether this can be achieved, or whether it is indeed a reasonable assumption, will be discussed in more depth in the pages to come), so that all time derivatives in Eqs.(3.1) cancel. Additionally, assuming spherical symmetry, Eqs.(3.1) reduce to two much simpler equations:

$$\frac{dP(r)}{dr} = -\rho(r)g(r) \,, \tag{3.2}$$

and:

$$\frac{d\Gamma_{\text{heat}}(r)}{dV} = \frac{d\Gamma_{\text{cool}}(r)}{dV} \,. \tag{3.3}$$

In Eq.(3.2), $g(r) = \nabla \phi$ is the local gravitational acceleration. Together with the pressure profile, $P(r)$, it can be related to the density profile $\rho(r)$ via the following:

$$g(r) = \frac{v_{\text{rot}}^2}{r} = \frac{G}{r^2} \int_0^r dr' \, 4\pi r'^2 \rho_T(r') \;\; ; \;\; P(r) = \frac{\rho(r)T(r)}{\overline{m}} \,, \tag{3.4}$$

having assumed local thermal equilibrium in relating P to T, with $\overline{m} = (n_{F_1}m_{F_1} + n_{F_2}m_{F_2})/(n_{F_1} + n_{F_2})$ being the mean mass of the dark plasma. In the above, $\rho_T(r)$ denotes the total mass density, thus comprehensive of dark plasma [with mass density $\rho(r)$], baryonic components (stars and gas) and possibly dark stars.

There are a few points worth commenting with respect to Eqs.(3.2,3.3). The former catches the eye as simply being the hydrostatic equilibrium equation. The latter is instead an energy

balance equation, with Γ_{cool} taking into account dissipative interactions (the details of which are determined by the particle physics underlying our model), and Γ_{heat} encoding the heating of the halo which takes place through dark photons, originating from kinetic mixing induced processes within the core of ordinary supernovae. Both hydrostatic equilibrium and energy balance are required for a static configuration to be achieved.

One can legitimately raise the question as to whether the system can actually reach a static configuration; we believe this is possible, if not fairly plausible. Let us assume that at an earlier time, prior to ordinary star formation, the system was in a more compact arrangement. The star formation activity that would follow is expected to heat the halo, so that $\Delta\Gamma = \Gamma_{\text{heat}} - \Gamma_{\text{cool}} > 0$ initially. As the halo expands, a series of feedback processes are expected to modify $\Delta\Gamma$, until the equilibrium situation $\Delta\Gamma = 0$ is achieved. As an example of what such a feedback mechanism might be, the weakening gravity which follows from the expansion of the halo causes a reduction in the star formation rate, $\dot{\Sigma}_\star$, and hence in the supernovae rate, as is expressed by the Schmidt-Kennicutt empirical law [70]:

$$\dot{\Sigma}_\star \propto n_{\text{gas}}^N \,, \ N \sim 1 - 2 \,. \tag{3.5}$$

There are other processes which could work in the same direction as the above, that is, leading to a net reduction in $\Delta\Gamma$ as the halo expands, and a net increase in $\Delta\Gamma$ when the halo contracts, until finally $\Delta\Gamma = 0$ is reached.[2]

To acquire some preliminary insight, we now solve the hydrostatic equilibrium equation [Eq.(3.2)] assuming an isothermal halo, i.e. $dT/dr = 0$, and making the approximation $\rho_T(r) = \rho(r)$. In the outskirts of the galaxy, where the dark matter component dominates over the baryons, both approximations are reasonable. Combining Eqs.(3.2,3.4) and using the isothermal approximation, we can express the hydrostatic equilibrium equation in the following form:

$$\frac{d\rho}{dr} = -\frac{\overline{m}\rho(r)G}{Tr^2} \int_0^r dr' 4\pi r'^2 \rho(r') \,. \tag{3.6}$$

We solve Eq.(3.6) by a polynomial of the form $\rho = \lambda/r^p$, from which we obtain $p = 2$ and $\lambda = T/2\pi G\overline{m}$, and hence:

$$\rho(r) = \frac{T}{2\pi G\overline{m}r^2} \,. \tag{3.7}$$

Combining Eqs.(3.4,3.7) results in a relation between the rotational velocity profile and the temperature of the halo:

$$v_{\text{rot}}^2 = \frac{G}{r} \int_0^r dr' \ 4\pi r'^2 \frac{T}{2\pi G\overline{m}r'^2} = \frac{2T}{\overline{m}} \implies T = \frac{1}{2}\overline{m}v_{\text{rot}}^2 \equiv \frac{1}{2}\overline{m}v_\infty^2 \,. \tag{3.8}$$

Accordingly, we find that the rotational velocity is constant at a value v_∞ (the asymptotic rotational velocity), in agreement with the asymptotically flat rotational curves of spiral galaxies.

3.1.1 Toy model

As we have just determined, the approximation of an isothermal halo has allowed us to solve the hydrostatic equilibrium equation. One is obviously brought to question whether

---

[2]As another example, as the halo expands, the less dense plasma becomes more optically thin to the heating dark photons; these then find it easier to escape, decreasing the heating rate.

such an approximation is in fact justified. To address this issue, we now expose how, within the assumption of an isothermal halo, not only can we solve the hydrostatic equilibrium equation, but also satisfy the energy balance condition. We consider a toy model, in which all supernovae act as a point source located at the galactic centre and produce a total dark photon luminosity L_{SN}. Applying the energy balance condition requires being able to express the energies absorbed and dissipated within a volume element dV, and subsequently matching them.

We make the assumption that thermal dark bremsstrahlung of F_1 off F_2 is the main dissipation avenue. The dark photons radiated can escape and hence cool the halo. We do not consider bremsstrahlung of F_1 off itself (or of F_2 off itself, for that matter) since it is well known that, in the dipole approximation, the amplitude for bremsstrahlung of a particle off itself is zero (see e.g. [71] for more thorough discussions). Under this assumption, the energy dissipated per unit time within a volume element dV is given by:

$$d\Gamma_{cool} = \Lambda(T) n_{F_1} n_{F_2} dV , \qquad (3.9)$$

where $\Lambda(T)$ is the cooling function for bremsstrahlung ($\Lambda(T) \propto \sqrt{T}$, see e.g. [71]) and from here on n_{F_1} will denote the number density of free F_1 particles. Two remarks are in order at this point. *In primis*, other cooling mechanisms which could be important sources of dissipation can be considered: for instance, line emission, recombination and inverse dark Compton scattering. Their effect can be taken into account simply by modifying $\Lambda(T)$.[3] Further, a more exhaustive analysis of the cooling process would have to account for the fact that not all dark photons have sufficient mean free path so as to escape the halo and contribute to cooling. This effect can be modelled by means of a cooling efficiency, which is a function of both the wavelength and the location of the dark photons in the halo. For the sake of simplicity, we shall neglect the complications mentioned above, which anyhow are not crucial for our discussions.

As outlined previously, the ultimate effect of kinetic mixing induced processes within the core of ordinary supernovae is to reprocess $\lesssim 1/2$ of the core-collapse energy into dark photons (whose spectrum is of course uncertain) in the region surrounding the supernovae. The end result is that these dark photons can carry away a considerable amount of energy, which is then injected into the halo via heating mechanisms to be discussed here. One can in principle consider two suitable mechanisms: dark photoionization and dark Thomson scattering. In Appendix A we demonstrate that dark Thomson scattering is an efficient heating mechanism only for $m_{F_1} \lesssim 0.1$ MeV, which is outside of the range of parameter space we are considering (refer to Chapter 2). This happens because dark Thomson scattering, in addition to being kinematically inefficient, has a cross-section which is too small. The end result is that, for the range of parameter space we are exploring, only dark photoionization is expected to be an important heating process.

Two notes of caution are needed here: for dark photoionization to occur, we have to assume that the two K-shell F_1 states are occupied, and hence the plasma will not be completely ionized. At the one and only scope of simplicity, we will assume that the remaining $(|Z'|-2)$ F_1 states are free, leaving the discussion of consistency conditions which are hereby implied for later discussion. Finally, the requirement that the two K-shell F_1 states be occupied, in addition with the requirement that the plasma be partially ionized, clearly requires that $|Z'| \geq 3$. Having made these preliminary considerations, we can now express the energy being absorbed per unit time within a volume element dV via dark photoionization, whose

---

[3]In the case of inverse dark Compton scattering, $F_1\gamma_D \to F_1\gamma_D$ (where γ_D is a dark microwave background [dark!] photon) we find that such a process can be safely neglected, given the examined range of paramer space and physical conditions. This, however, ceases to be true at an earlier epoch, $z \gtrsim 3$.

cross-section is σ_{DP} (see e.g. [30]):

$$d\Gamma_{\text{heat}} = \frac{L_{\text{SN}}e^{-\tau}}{4\pi r^2}\sigma_{DP}n_{F_2}dV \, , \tag{3.10}$$

where τ is the optical depth. In principle we would have to integrate over the (unknown!) spectrum of dark photons. For the purpose of our discussion, this detail is not essential.

We are now ready to apply the energy balance equation. We do so by matching the heating and cooling rates given in Eqs.(3.9,3.10), which yields:

$$n_{F_1} = \frac{L_{\text{SN}}e^{-\tau}}{\Lambda(T)4\pi r^2}\sigma_{DP} \, . \tag{3.11}$$

Under the assumption of the halo being optically thin, that is, $\tau \ll 1$, we recover $n_{F_1} \propto 1/r^2$, from which $\rho \propto 1/r^2$ follows. This signifies that the isothermal halo approximation is simultaneously a solution to the energy balance and hydrostatic equilibrium conditions. In essence, at large distances from the galactic centre, where the supernova heat source can be described as a point source and $\rho_T(r) \simeq \rho(r)$, the isothermal approximation is a reasonable one, as foreseen.

3.1.2 A more realistic model: solution to the core-cusp problem

Although the toy model did a good job in solving the equations of hydrostatic equilibrium and energy balance, it presents a weakness that should not be overlooked: it is clearly unphysical at $r = 0$. While approximating the supernova heat source as a point source is justified in the outskirts of the galaxy, this is certainly not the case in the proximity of the galactic centre! We here seek to describe the supernova distribution within the galaxy in a manner which is both simple and does not incur into problems as per above. It is not unreasonable to presume that such a heat source has a similar distribution to the mass of the galactic disk. In the end, it is dying stars (which reside in the galactic disk) that we are dealing with. If this is the case, we would expect the $\rho \propto 1/r^2$ solution to hold only far from the galactic centre, that is, for $r \gg r_D$.

To proceed, we approximate the mass of the galactic disk by a Freeman disk profile, whose surface density is given by [72]

$$\Sigma(\widetilde{r}) = \frac{m_D}{2\pi r_D^2}e^{-\frac{\widetilde{r}}{r_D}} \, , \tag{3.12}$$

where r_D and m_D are the length scale and the total mass of the disk respectively. We employ cylindrical coordinates $(\widetilde{r}, \widetilde{\theta}, \widetilde{z})$, with the galactic disk residing at $\widetilde{z} = 0$. It then follows that the flux at a point $P = (r_1, 0, z_1)$, for an optically thin halo, is given by (see e.g. [30]):

$$f(r, \cos\phi) = \frac{L_{\text{SN}}}{4\pi m_D}\int d\widetilde{\theta}\int d\widetilde{r}\,\widetilde{r}\frac{\Sigma(\widetilde{r})}{\widetilde{r}^2 - 2\widetilde{r}r_1\cos\widetilde{\theta} + r_1^2 + z_1^2} \, , \tag{3.13}$$

with $r = \sqrt{r_1^2 + z_1^2}$ and $\cos\phi \equiv r_1/r$. One can show that:

$$f(r, \cos\phi) \sim \begin{cases} \log r, & r \lesssim r_D \, , \\ \frac{1}{r^2}, & r \gg r_D \, . \end{cases} \tag{3.14}$$

In this more realistic model, the energy absorbed per unit time within a volume element dV is given by:

$$d\Gamma_{\text{heat}} = f(r, \cos\phi)\sigma_{DP}n_{F_2}dV \, , \tag{3.15}$$

29

while the energy dissipated per unit time within the same volume element via thermal dark bremsstrahlung is still given by Eq.(3.9).

Imposing the energy balance condition, and hence equating Eqs.(3.9,3.15), it follows that $n_{F_1} = f(r, \cos \phi)\sigma_{DP}/\Lambda(T)$, which in turn implies that $\rho \propto f(r, \cos \phi)$. The behavior of $f(r, \cos \phi)$ [Eq.(3.14)] suggests that we can approximate $\rho(r)$ by means of a quasi-isothermal profile:

$$\rho(r) \simeq \frac{\rho_0 r_0^2}{r^2 + r_0^2} \, , \tag{3.16}$$

where $r_0 \sim r_D$, given that r_D is the only length scale which is present. This scaling relation is indeed implied by measurements of high-resolution rotation curves, which found [73]:

$$\log r_0 = (1.05 \pm 0.11)r_D + (0.33 \pm 0.04) \, . \tag{3.17}$$

In Figure 3.1 we compare the radial dependence of the solution $\rho \propto f(r, \cos \phi)$, the quasi-isothermal profile given by Eq.(3.16) and a $\rho \propto 1/r^2$ profile. We find good agreement between the first two up to a scale $r \simeq r_D$. Below this scale (that is, approaching the galactic center), baryonic physics plays a dominant role in the dynamics being discussed and it is not possible to further understand the physics governing the density profile without prior appropriate modelling of the baryons.
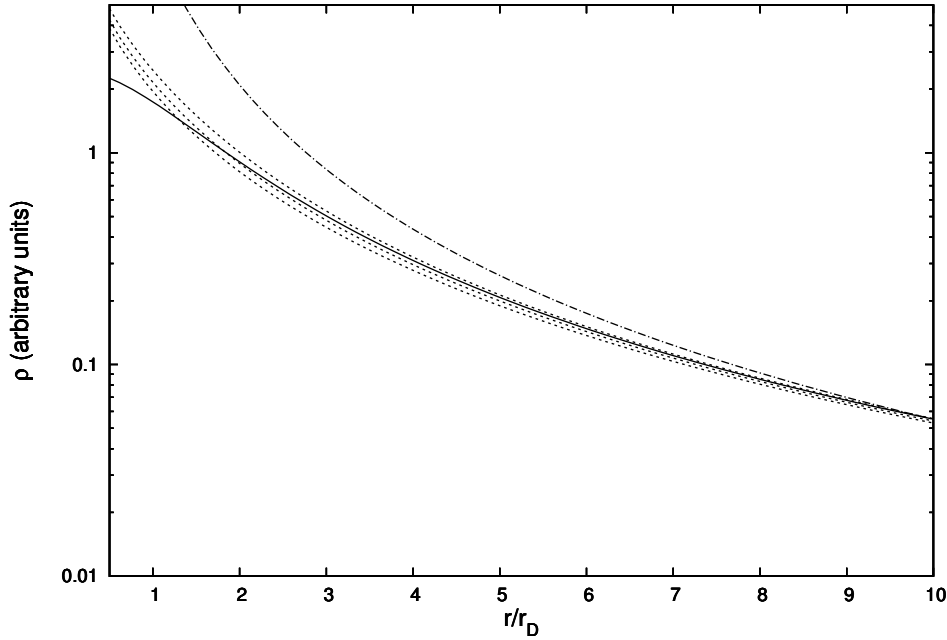

Figure 3.1: Comparison between the radial dependence of $\rho \propto f(r, \cos \phi)$, the quasi-isothermal profile given by Eq.(3.16), and a cuspy profile $\rho \propto 1/r^2$ (in arbitrary units). The dotted lines correspond to $f(r, \cos \phi)$ for (going from upper to lower line) $\phi = \pi/4, \pi/3, \pi/2$. The solid line corresponds to a cored density profile (with $r_0/r_D = 1.4$), while the dot-dashed line corresponds to the cuspy profile.

An observation is necessary at this stage: the profile obtained in Eq.(3.16) is cored and not cuspy ($\rho \propto 1/r^2$). The core arises because the supernova heat source has been smeared over a finite volume, rather than being treated as an unphysical point source. As we explicated in Chapter 1, the presence of cores in the halos of spiral galaxies has been inferred by a number of observations, whereas collisionless CDM simulations appears unable to account for such a cored profile, predicting a cuspy one instead. Whether the profile is actually cored is still

argument of debate; nevertheless, the fact that observations reveal a dark matter density profile towards the center of spiral galaxies which is lower than what current collisionless CDM simulations predict is undeniable [12].

Astroparticle physicists typically bring back this reduction in the dark matter density profile to two possible explanations: self-interactions between dark matter particles (which collisionless CDM cannot encompass), which are expected to redistribute the energy equally among these particles towards the center of the galaxy; and baryonic feedback mechanisms, although rarely is it gone into depth as to discussing what exactly such mechanism might be. In our work we have shown how the approach adopted by these two explanations is indeed a well-founded possibility, and have specified an exact feedback mechanism too: self-interactions, although not redistributing the energy in question, contribute to its dissipation; baryonic feedback processes, arising from core-collapse supernovae, supply the energy lost to the aforementioned dissipative self-interactions. The end result is that the dark matter density profile is lower than that predicted by collisionless CDM, consistent with observations.

So far, we have only made use of the requirement that energy balance hold within a given spiral galaxy. We have yet to exploit the fact that the energy balance condition is to hold for every spiral galaxy. Given that the heating rate is proportional to the supernovae rate and the cooling rate is related to properties of the dark matter halo (ρ_0 and r_0, for instance), we anticipate that the energy balance condition will suggests a connection between the baryonic and dark matter components within spiral galaxies. As we will see shortly, it will indeed result in a scaling relation which has been observed to hold for some time now, but has never been properly explained and has remained somewhat mysterious.[4]

3.1.3 Tully-Fisher relation

Let us now require that the energy balance condition holds for every spiral galaxy. The differential cooling rate has been expressed in Eq.(3.9), which in a moment we will proceed to integrate. As anticipated, the cooling rate is expected to depend on the parameters defining the dark matter density profile, that is, ρ_0 and r_0. This happens because the density profile, ρ, can be related to the the F_1 and F_2 number densities [which appear in Eq.(3.9)] via:

$$\rho = n_{F_2}(m_{F_2} + |Z'|m_{F_1}) \equiv \frac{n_{F_2}}{\kappa} . \tag{3.18}$$

Hence, under the assumption that the plasma is not fully ionized but retains its K-shell F_1 states (in order for dark photoionization to occur), we have that $n_{F_1} \approx \rho\kappa(|Z'| - 2)$ and $n_{F_2} = \rho\kappa$.[5] Integrating Eq.(3.9) and bearing in mind the previous observations results in:

$$\Gamma_{\text{cool}} = \Lambda(T)\kappa^2(|Z'| - 2)\rho_0^2 r_0^4 \int_0^\infty dr' \frac{4\pi r'^2}{(r'^2 + r_0^2)^2} = \pi^2\kappa^2(|Z'| - 2)\Lambda(T)\rho_0^2 r_0^3 . \tag{3.19}$$

For the purpose of the coming discussion, explicitly writing out $\Lambda(T)$ will not be necessary. One just needs note that, assuming the main dissipation route being thermal dark bremsstrahlung, $\Lambda(T) \propto \sqrt{T} \propto v_\infty$, where we have related the temperature T to the rotational velocity far from the galactic center, v_∞, via Eq.(3.8) (the reason why we choose to express the dependence on the asymptotic rotational velocity will be appreciated shortly). If we neglect

---

[4]Hopefully the reader will feel otherwise in this respect after reading the following section.

[5]In order to account for partial ionization of the remaining atomic states, we could write in a more general way $n_{F_1} = f\rho\kappa(|Z'| - 2)$, with $f \leq 1$.

baryonic contributions, the rotational velocity profile, $v_{\text{rot}}(r)$, can be related to the quantities defining the dark matter density profile, ρ_0 and r_0, via Eq.(3.4):

$$v_{\text{rot}}^2 = \frac{G}{r} \int_0^r dr' \, 4\pi r'^2 \frac{\rho_0 r_0^2}{r'^2 + r_0^2} = 4\pi G \rho_0 r_0^2 \left[1 - \frac{r_0}{r} \tan^{-1}\left(\frac{r}{r_0}\right) \right] , \tag{3.20}$$

from which we obtain that the asymptotic rotational velocity ($r \gg r_D \sim r_0$) is:

$$v_\infty = 2\sqrt{\pi G \rho_0 r_0^2} . \tag{3.21}$$

We now proceed to express the heating rate, which is proportional to the supernovae rate, and hence to properties of the baryonic component. For a given spiral galaxy, the heating rate is given by:

$$\Gamma_{\text{heat}} = f_{\text{SN}} \langle E_{\text{SN}} \rangle R_{\text{SN}} , \tag{3.22}$$

where f_{SN} is the fraction of the total energy output which is absorbed by the halo and E_{SN} is the total energy output from each supernova, which occur at a rate given by R_{SN}. It is useful to relate f_{SN} to the relevant optical depth, via:

$$f_{\text{SN}} = R_{\gamma_D} \langle (1 - e^{-\tau}) \rangle . \tag{3.23}$$

Here $R_{\gamma_D} \equiv E_D / E_{\text{SN}}$ is the fraction of the total supernova energy output which is converted into dark particles (where E_D is the *quota* of energy released from the supernova which is converted into creation of dark photons). To obtain a measure of the average optical depth, let us consider dark photons propagating from the galactic center to the edge of the galaxy (which we approximate as $r \to \infty$):

$$\tau = \int_0^\infty dr \, \sigma_{DP} n_{F_2} = \int_0^\infty dr \, \sigma_{DP} \rho \kappa = \frac{\pi \sigma_{DP} \kappa \rho_0 r_0}{2} . \tag{3.24}$$

For an optically thin halo (that is, for $\tau \ll 1$), combining Eqs.(3.18,3.22,3.23,3.24) results in the following expression for the total heating rate:

$$\Gamma_{\text{heat}} = \frac{\pi R_{\gamma_D} \sigma_{DP} \kappa \langle E_{\text{SN}} \rangle}{2} \rho_0 r_0 R_{\text{SN}} . \tag{3.25}$$

We now enforce the energy balance condition, and hence equate Γ_{cool} [Eq.(3.19)] and Γ_{heat} [Eq.(3.25)], yielding:

$$R_{\text{SN}} = \frac{2\pi \kappa (|Z'| - 2)}{R_{\gamma_D} \sigma_{DP} \langle E_{\text{SN}} \rangle} \Lambda(T) \rho_0 r_0^2 . \tag{3.26}$$

As forecasted, we have extracted a scaling relation connecting baryonic properties (via R_{SN}) to dark matter properties (via ρ_0, r_0), which is independent of the one obtained earlier, $r_0 \sim r_D$. Aside from the numerical factors at the front, the genuinely interesting aspect of this scaling relation is $R_{\text{SN}} \propto \Lambda(T) \rho_0 r_0^2$, where $\Lambda(T) \propto v_\infty \propto (\rho_0 r_0^2)^{\frac{1}{2}}$. It follows that we can express Eq.(3.26) as a relation connecting the supernovae rate to the asymptotic rotational velocity for every (emphasis on "every"!) spiral galaxy:

$$R_{\text{SN}} \propto v_\infty^3 . \tag{3.27}$$

To better appreciate what we have obtained, let us note that observational studies on supernovae have related the supernovae rate to the B-band luminosity of the respective spiral galaxy, via $R_{SN} \propto (L_B)^{0.73}$ [74] which, combined with Eq.(3.27), gives:

$$L_B \propto v_\infty^4 \ . \tag{3.28}$$

The scaling relation we have just written down is better known as the *Tully-Fisher relation* (TFR hereafter). The TFR is an empirical relation that is observed to hold for all spiral galaxies and finds a very useful application in astronomy, where it is used to measure the distance to galaxies up to ~ 100 Mpc away from us (see e.g. [69]). The general form of the Tully-Fisher relation is $L \propto (v_\infty)^\alpha$, where α depends on the bandpass through which the luminosity is measured. For instance, for the K-band (near-infrared) $\alpha = 4.35 \pm 0.14$ has been measured, while for the optical B-band (which we have used above) $\alpha = 3.91 \pm 0.13$ has been found [75]. The scaling relation we have derived is consistent with the value of α measured, within error bars. This is really exciting, given that the TFR, as it stands, is unexplained, despite the fact that most astrophysicists believe it suggests a deep connection between baryonic and dark matter components in spiral galaxies. The model we have provided implements such a connection explicitly by means of the nontrivial dissipative dynamics at play. The TFR is equivalent to the energy balance condition: Γ_{heat} arises from supernovae heating and Γ_{cool} from dissipative dynamics, inherent to our particle model for dark matter. This picture is expected to hold within all galaxies that have ongoing star formation, and hence among irregular galaxies as well.

As a final remark, we elucidate how this model can explain another puzzling observational feature of spiral galaxies: the product of the inferred core densities and radii of dark matter halos is roughly constant, that is, $\rho_0 r_0 \approx$ const [76]. Note however that this scaling relation is not independent of the two previously determined ($r_0 \sim r_D$ and the TFR). To see how this scaling relation can be obtained, recall the TFR: $L_B \propto (v_\infty)^4 \propto \rho_0^2 r_0^4$. Observational studies of spiral galaxies have obtained the scaling relations $m_D \propto (L_B)^{1.3}$ [77] and $r_D \propto (m_D)^{0.38}$ [78]. Combining these four relations one easily obtains $\rho_0 r_0 \approx$ const, *quod erat demonstrandum*.

3.1.4 Elliptical galaxies: the Faber-Jackson relation

What about elliptical galaxies? Is our model capable of addressing some of their unusual properties? Ellipticals, unlike spirals, are significantly more tridimensional (with the motion of the stars being mostly radial, rather than circular), and contain a considerable amount of dark matter. But their most bizarre property is the fact that they are almost entirely devoid of interstellar matter, that is, they possess almost no baryonic matter or dust. Unsurprisingly, then, elliptical galaxies are inhabited by very few young stars, and have a very low star formation rate. Their population is made up predominantly of old, low-mass stars, and they are typically surrounded by several globular clusters.

The suppressed star formation rate implies that the dynamical halo model formulated for spiral (and irregular) galaxies does not appear to be viable here. To make progress, it might be useful to speculate as to the origin of elliptical galaxies. The commonly accepted (but by no means final) picture regarding the formation of elliptical galaxies sees them as the result of a merger of spiral galaxies. We will here take a more unconventional stand and claim that it is instead possible for ellipticals to represent the final evolutionary stage of spirals. Some time into their evolution, spirals are expected to exhaust their baryonic gas, meaning that the ordinary supernovae rate is no more sufficient to support the dark matter halo against cooling. Let us now conjecture as to what this might mean in terms of the future evolution of this (by now dead?) spiral.

Denoting by t_{cool} and t_{ff} the cooling and free-fall timescales for the dark matter halo, we will now consider the limiting case where $t_{cool} \ll t_{ff}$. Under this assumption, it is possible for the dark matter halo to cool, and potentially fragment into dark stars. When the heating has stopped and the halo has begun to cool (but not collapse), we can approximate its total energy as being solely the gravitational potential energy, since the velocity dispersion of the dark matter particles is now negligible:

$$U_i = -\int_0^R dr\, 4\pi r^2 \frac{GM_r}{r} \rho(r) \simeq -4\pi\rho_0 r_0^2 GM_t \,, \tag{3.29}$$

where $M_r = \int_0^r dr'\, 4\pi r'^2 \rho(r') \simeq 4\pi\rho_0 r_0^2 r$ is the mass enclosed within a radius r and $M_t = \int_0^R dr\, 4\pi r^2 \rho(r) \simeq 4\pi\rho_0 r_0^2 R$ is the total mass. In evaluating the relevant integrals above, we have made use of the density profile given by Eq.(3.16), which is justified since the limit we are considering ($t_{cool} \ll t_{ff}$) does not allow for sufficient "time" for the dark matter halo to change.

At this point the system can begin to contract and eventually form dark stars. If this occurs, two events are expected to take place here. To begin with, dark stars can eventually produce dark supernovae. Via kinetic mixing induced processes (proceeding the other way round, this time!), these dark supernovae will convert a significant fraction of their core-collapse energy into ordinary photons, which could not only heat the ordinary matter, but also blow it out of the galaxy. This might potentially explain both why there is so little baryonic gas in ellipticals and why the little gas that is present appears to be distributed in three dimensions rather than as a flat disk as it would be in spirals. Next, the newly formed dark stars will fall into the gravitational well as the system contracts. In doing so they attain kinetic energy, and hence velocity dispersion. Their final kinetic energy, T_f, can be related to the final potential energy, U_f, via the virial theorem, which states that $U_f = -2T_f$. Conservation of energy implies that $U_i = U_f + T_f = -T_f$ [with U_i given by Eq.(3.29)], and hence expressing T_f in terms of the dark star velocity dispersion σ via $T_f = 3M_t\sigma^2/2$, we obtain:

$$\sigma^2 = \frac{8\pi G\rho_0 r_0^2}{3} \,. \tag{3.30}$$

If we now make a more bold assumption, namely that the ordinary stars thermalize with the dark ones, it follows that their velocity dispersion too is σ. In addition, given that the now elliptical has evolved from a spiral, the parameters ρ_0 and r_0 will still obey the scaling relations previously deduced. By using $\rho_0 r_0 \approx$ const and $r_0 \sim r_D \propto \sqrt{L_B}$, which has been derived from the previous $m_D \propto (L_B)^{1.3}$ [77] and $r_D \propto (m_D)^{0.38}$ [78], we infer a scaling relation connecting the B-band luminosity of the newly formed elliptical galaxy with the velocity dispersion of its stars:

$$L_B \propto \sigma^4 \,. \tag{3.31}$$

The above [Eq.(3.31)] is known as *Faber-Jackson relation* [79], and is very similar in form to the TFR. It is observed to hold for elliptical galaxies, and is part of a series of empirical correlations known as the *fundamental plane*.

3.2 Consistency conditions and energy balance

In the preceding sections we have derived scaling relations which connect the baryonic and dark matter components in spiral galaxies, building on the assumption that the system

evolves to a static configuration, which translates to an energy balance condition. The baryonic properties were encoded in R_{SN} (or equivalently L_B), while the dark matter properties were described by ρ_0 and r_0. On the other hand, there are other parameters still which characterize the dark matter properties; that is, the 5 parameters of our dark matter particle model: m_{F_1}, m_{F_2}, α', ϵ and Z'. Our next objective is then to understand how the energy balance argument can constrain the relevant parameter space in question.

Let us start by re-examining the cooling rate [Eq.(3.19)]. To make further progress, we have to display the explicit dependence of the cooling function on the 5 parameters of the underlying dark matter model. Under the assumption of thermal dark bremsstrahlung of F_1 off F_2 being the preeminent dissipation mechanism, the energy lost per unit time per unit volume is given in e.g. [71] and is:

$$\frac{d\Gamma_{\text{cool}}}{dV} = 16\alpha'^3 \sqrt{\frac{2\pi T}{27 m_{F_1}^3}} Z'^2 n_{F_1} n_{F_2} \overline{g}_B \,, \tag{3.32}$$

where $\overline{g}_B \simeq 1.2$ is the frequency average of the velocity-averaged Gaunt factor for thermal bremsstrahlung. The temperature, T, is related to both the mean mass of the dark plasma and the asymptotic rotational velocity, v_∞. Working in the limit where $m_{F_2} \gg m_{F_1}$ and assuming neutrality of the plasma so that $n_{F_1} = (|Z'| - 2)n_{F_2}$ holds, we can make the approximation:

$$\overline{m} = \frac{n_{F_1} m_{F_1} + n_{F_2} m_{F_2}}{n_{F_1} + n_{F_2}} \approx \frac{m_{F_2}}{|Z'| - 1} \,. \tag{3.33}$$

Using Eqs.(3.8,3.16,3.18,3.21,3.32,3.33) then results in the total cooling rate being:

$$\Gamma_{\text{cool}} = 32\pi^3 \overline{g}_B \alpha'^3 Z'^2 (|Z'| - 2)\kappa^2 \sqrt{\frac{G m_{F_2}}{27(|Z'| - 1)m_{F_1}^3}} (\rho_0 r_0)^{\frac{5}{2}} r_0^{\frac{3}{2}} \,. \tag{3.34}$$

Concerning the heating mechanism, as explained previously, only dark photoionization is expected to be important for the range of parameter space we are considering. Dark photoionization is possible if the dark bound state (D^0), albeit being close to fully ionized, retains its K-shell F_1 atomic states. This is, of course, completely analogous to the MDM case where the heating of the halo occurs via photoionization of the K-shell mirror electrons of a mirror metal component. The cross-section for dark photoionization, σ_{DP}, can easily be obtained by adapting that for ordinary photoionization (which can be found in e.g. [71]):[6]

$$\sigma_{DP} = \frac{g' 16\sqrt{2}\pi}{3 m_{F_1}^2} \alpha'^6 |Z'|^5 \left(\frac{m_{F_1}}{E_{\gamma_D}}\right)^{\frac{7}{2}} \,. \tag{3.35}$$

3.2.1 Cooling timescale

The validity of the picture presented earlier calls for a series of consistency conditions to hold, which we now discuss before specifying in what way they constrain the relevant available parameter space. The first of these conditions is related to the halo cooling timescale. If such a timescale were larger than the Hubble time, clearly our dynamical equilibrium picture would have to be modified. For instance, the required heating rate would be diminished. From Eq.(3.34), recalling that $\kappa = (m_{F_2} + |Z'|m_{F_1})^{-1}$, it is straightforward to see that this requirement sets an upper bound on the allowed mass of the F_2 particle. Let us now derive the cooling timescale, t_{cool}. If we denote by n_T the total number density of dark particles,

---

[6]The quantity $g' = 1, 2$ counts the number of K-shell F_1 atomic states present.

$\mathcal{E} = 3n_T T/2$ and $\dot{\mathcal{E}} = \Lambda(T)n_{F_1}n_{F_2}$, the cooling timescale is given by $t_{\text{cool}} = \mathcal{E}/\dot{\mathcal{E}}$. If, in addition, we make the approximation $n_T \approx n_{F_1}$, we obtain:

$$t_{\text{cool}} \approx \frac{3T}{2\Lambda(T)n_{F_2}} \approx \frac{9}{64\bar{g}_B} \sqrt{\frac{3m_{F_2}m_{F_1}^3}{\pi(|Z'|-1)}} \frac{v_\infty}{\kappa\rho\alpha'^3 Z'^2} . \tag{3.36}$$

The cooling time displays a dependence on position, r, through the dependence on $\rho(r)$. Since less dense regions cool more slowly, the most stringent limit we can obtain will arise from regions where $\rho(r)$ is lowest, that is, in the outskirts of the galaxy. On the other hand, our knowledge of the properties of the dark matter halo far from the galactic center is limited, and hence we cannot push ourselves too far. As a compromise, we will obtain an upper limit on the mass of the F_2 particle by requiring that $t_{\text{cool}} \lesssim$ few billion years for $r \lesssim r_{\text{opt}}$, where $r_{\text{opt}} \approx 3.2r_D \sim 2r_0$ is the optical radius, within which the majority of the baryons reside (see e.g. [80]). Hence we will obtain the most stringent limit for $\rho(r \approx 2r_0) \approx \rho_0/5$. From Eq.(3.36) the reader can also infer that the most rigid bound (i.e. the longest cooling time) stems from the largest spiral galaxies, for whom $v_\infty \approx 300$ km/s. In the following we assume typical values for large spiral galaxies of $\rho_0 r_0 \simeq 100$ $M_\odot/\text{pc}^2$ and $r_0 \simeq 20$ kpc, from which $\rho_0/5 \simeq 10^{-3}$ $M_\odot/\text{pc}^3$. Requiring $t_{\text{cool}}(r \simeq 2r_0) \lesssim$ few billion years then yields the following upper limit:

$$m_{F_2} \lesssim 200 \left(\frac{\text{MeV}}{m_{F_1}}\right) \left(\frac{\alpha'}{10^{-2}}\right)^2 \left(\frac{|Z'|}{10}\right)^{\frac{5}{3}} \text{GeV} . \tag{3.37}$$

3.2.2 Ionization state of the halo

The dynamical halo model, governed by a balance between heating and cooling, built on two additional vital assumptions. First off, the halo is assumed to be ionized, that is, at least one free F_1 particle per (partially ionized) bound state. This requirement allows for efficient cooling via thermal dark bremsstrahlung, and sets a lower bound on the temperature of the halo. On the other hand, that D^0 retain its K-shell F_1 particles is the *conditio sine qua non* for adequate heating to take place via dark photoionization. This condition sets an upper bound on the same temperature.

In addition, we require that the two conditions outlined above hold for all spiral galaxies. That is, the dark plasma of the halo in all spirals is required to be in similar ionization states, regardless of the size of the galaxy. Why so? Because the physics of our model depends strongly on the fact that such particular ionization state be attained, so as to allow for the dynamical picture of balance between heating and cooling (from which, recall, the most important results and scaling relations were obtained) to be viable. If, say, only the biggest spirals were ionized ($T \propto v_\infty^2$ is greater for bigger spirals), we would expect sudden sharp observational differences in moving along the spectrum of spiral galaxies, with a cut-off at the scale for which the transition between two different ionization states occurs.

The transition between two ionization states, given the relevant ionization energy $\mathcal{I}$, occurs at a temperature $T = \mathcal{I}/\xi$, where recall $T = \bar{m}v_\infty^2/2 \approx m_{F_2}v_\infty^2/[2(|Z'|-1)]$. The value ξ assumes is fairly dependent on the parameters in question, and hence there will be a range of possible values for ξ. The exact details of such a calculation, which we carried out in [1], are not essential for our discussion, so we refer the reader to Appendix A of [1] should he wish to find out more. There we estimated that for the transition from a neutral to an ionized halo (at an ionization energy $\mathcal{I}$, and which allows us to set a lower bound on the mass of the F_2 particle), $\xi \approx 7-28$. A simple glance at the relevant equations [Eqs.(3.38)] shows us that in order to obtain a conservative lower bound on the mass of the F_2 particle we are

interested in the maximum value ξ can assume, $\xi_{\max} \approx 28$. On a similar note, when working out an upper bound on the mass of the F_2 particle, which is determined by the process of K-shell photoionization (with ionization energy $\mathcal{J}$), we require the minimum value ξ can obtain in relation to this process (which is slightly different to that of D^0 ionization, given that the central F_2 particle is almost unshielded!). In the same Appendix we estimate this to be $\xi_{\min} \approx \min[1/(\alpha'^3 Z'^4), 1]$. The gist of this lengthy discussion is that demanding all spirals share a similar ionization state corresponds to the following requirements:

$$T \gtrsim \frac{\mathcal{I}}{\xi_{\max}} \quad \implies \quad \frac{m_{F_2}}{\text{GeV}} \gtrsim \left(\frac{|Z'|}{10}\right)\left(\frac{\alpha'}{10^{-2}}\right)^2\left(\frac{m_{F_1}}{\text{MeV}}\right)\left(\frac{50 \text{ km/s}}{v_\infty}\right)^2 ,$$

$$T \lesssim \frac{\mathcal{J}}{\xi_{\min}} \quad \implies \quad \frac{m_{F_2}}{\text{GeV}} \lesssim 100\left(\frac{|Z'|}{10}\right)^3\left(\frac{\alpha'}{10^{-2}}\right)^2\left(\frac{m_{F_1}}{\text{MeV}}\right)\left(\frac{300 \text{ km/s}}{v_\infty}\right)^2 g(\alpha', Z') , \qquad (3.38)$$

where $g(\alpha', Z') \equiv \max(\alpha'^3 Z'^4, 1)$. Noting that the bounds in Eq.(3.38) have to hold for all spirals, one grasps that the most stringent lower bound on the mass of the F_2 particle is set by the smallest spiral/irregular galaxies, for which $v_\infty \approx 50$ km/s, while the most stringent upper bound arises from the biggest spirals, with $v_\infty \approx 300$ km/s. Hence the bounds on m_{F_2} arising from ionization physics can be expressed in a more concise way as:

$$\left(\frac{|Z'|}{10}\right)\left(\frac{\alpha'}{10^{-2}}\right)^2\left(\frac{m_{F_1}}{\text{MeV}}\right) \lesssim \frac{m_{F_2}}{\text{GeV}} \lesssim 100\left(\frac{|Z'|}{10}\right)^3\left(\frac{\alpha'}{10^{-2}}\right)^2\left(\frac{m_{F_1}}{\text{MeV}}\right)g(\alpha', Z') . \qquad (3.39)$$

Let us note that it is possible for either or both the above inequalities to actually be equalities. In this case we are dealing with a limiting situation. That is, ionization physics could be responsible for establishing the scale of spiral and irregular galaxies (via $v_\infty^{\max}$, $v_\infty^{\min}$). This is a possible explanation for why both very big spirals and very small irregulars are not observed. If we equate the upper and lower bounds in Eq.(3.39) we obtain that this plight takes place for $|Z'| \sim 1$.

Prior to moving on, we here demand that the upper bound derived on the mass of the F_2 particle from the cooling timescale argument in Eq.(3.37) be greater than that derived from ionization physics arguments in Eqs.(3.38). Doing so results in most factors conveniently cancelling, leaving us with the following lower bound on the magnitude of the F_2 and F_1 charge ratio:

$$|Z'| \gtrsim 4\left(\frac{m_{F_1}}{10 \text{ MeV}}\right)^3 . \qquad (3.40)$$

3.2.3 Energy balance

Let us now return to the energy balance condition, that is, $\Gamma_{\text{heat}} = \Gamma_{\text{cool}}$. We have already derived the total cooling rate for the dark matter halo, under the assumption of the main dissipation path being thermal dark bremsstrahlung [Eq.(3.34)]. A complete understanding of the heating rate is actually a very complicated matter. The issue here is that one would have to integrate over the spectrum of dark photons which arise from kinetic mixing induced processes in the core of ordinary supernovae and, it is professed, heat the dark matter halo. Of course, such a spectrum is unknown, and is very hard to predict![7] Here we simply observe that we can set an upper limit on the heating rate:

$$\Gamma_{\text{heat}} \lesssim R_{\gamma_D} R_{\text{SN}} \langle E_{\text{SN}} \rangle \min(\tau_{\max}, 1) . \qquad (3.41)$$

---

[7]In the framework of MDM work has been done parametrizing such spectrum via a power law and a cut-off energy somewhat higher than the binding energy of the K-shell mirror electron of the relevant mirror metal component. This approach is somewhat justified by observing that the behavior of the photoionization cross-section with energy ($\sigma \propto E^{-7/2}$) suggests that it is mainly the low energy part of the spectrum that contributes to the heating of the halo [30].

In the above, $\tau_{\max}$ is the maximum value the optical depth [Eq.(3.24)] can assume, having allowed for all possible forms for the spectrum of dark photons. Eq.(3.24), jointly with Eq.(3.35), suggests that the optical depth assumes its maximum value when the dark photon energy is the lowest possible. That is, when $E_{\gamma_D} = I'$, where $I' \approx Z'^2 \alpha'^2 m_{F_1}/2$ is the binding energy of the relevant K-shell F_1 particle. In this case we obtain:

$$\tau_{\max} = \frac{256\pi^2}{3} \frac{\rho_0 r_0}{m_{F_1}^2 m_{F_2} \alpha' Z'^2} \gtrsim 40 \left(\frac{\text{MeV}}{m_{F_1}}\right)^3 \left(\frac{10^{-2}}{\alpha'}\right)^3 \left(\frac{10}{|Z'|}\right)^5 \frac{1}{g(\alpha', Z')} , \qquad (3.42)$$

where in order to obtain the inequality we have exploited the fact that for spiral galaxies $\rho_0 r_0 \approx$ const, with an indicative value for this quantity being $\rho_0 r_0 \approx 100\ M_\odot/\text{pc}^2 \simeq 4.6 \times 10^{-6}\ \text{GeV}^3$, and additionally made use of the upper bound on m_{F_2} given in Eq.(3.39). Eq.(3.42) suggests that $\tau_{\max} \gtrsim 1$ should hold for an important fraction of parameter space.

For definiteness, we shall now assume parameters where $\tau_{\max} \gtrsim 1$ hold and estimate an upper limit for the heating rate, noting that this limit will hold even if $\tau_{\max} \lesssim 1$, since $\min(\tau_{\max}, 1) \leq 1$. In this case we would simply be assuming a more conservative position. The fraction of the total energy output in dark particles, R_{γ_D}, is a function of the kinetic mixing parameter, ϵ. For $\epsilon \lesssim 10^{-9}$, $R_{\gamma_D} \propto \epsilon^2$, while for $\epsilon \gtrsim 10^{-9}$, R_{γ_D} saturates at $\sim 1/2$ [37].[8] For $\epsilon \lesssim 10^{-9}$, inserting numbers into Eq.(3.41), we obtain the following upper limit on Γ_{heat}:

$$\Gamma_{\text{heat}} \lesssim 10^{44} \left(\frac{\epsilon}{10^{-9}}\right)^2 \left(\frac{\langle E_{\text{SN}} \rangle}{3 \times 10^{53}\text{erg}}\right) \left(\frac{R_{\text{SN}}}{0.03\ \text{yr}^{-1}}\right) \frac{\text{erg}}{\text{s}} . \qquad (3.43)$$

Doing the same for Γ_{cool} [Eq.(3.34)], we get:

$$\Gamma_{\text{cool}} \simeq 10^{44} \left(\frac{\alpha'}{10^{-2}}\right)^3 \left(\frac{\text{MeV}}{m_{F_1}}\right)^{\frac{3}{2}} \left(\frac{|Z'|}{10}\right)^{\frac{5}{2}} \left(\frac{10\ \text{GeV}}{m_{F_2}}\right)^{\frac{3}{2}} \left(\frac{\rho_0 r_0}{100\ \frac{M_\odot}{\text{pc}^2}}\right)^{\frac{5}{2}} \left(\frac{r_0}{5\ \text{kpc}}\right)^{\frac{3}{2}} \frac{\text{erg}}{\text{s}} . \qquad (3.44)$$

By comparing Eqs.(3.43,3.44), we note that the following approximate relation has to hold:

$$C \left(\frac{10^{-9}}{\epsilon}\right)^2 \left(\frac{\alpha'}{10^{-2}}\right)^3 \left(\frac{\text{MeV}}{m_{F_1}}\right)^{\frac{3}{2}} \left(\frac{|Z'|}{10}\right)^{\frac{5}{2}} \left(\frac{10\ \text{GeV}}{m_{F_2}}\right)^{\frac{3}{2}} \lesssim 1 , \qquad (3.45)$$

having defined:

$$C \equiv \left(\frac{\rho_0 r_0}{100\ \frac{M_\odot}{\text{pc}^2}}\right)^{\frac{5}{2}} \left(\frac{r_0}{5\ \text{kpc}}\right)^{\frac{3}{2}} \left(\frac{3 \times 10^{53}\ \text{erg}}{\langle E_{\text{SN}} \rangle}\right) \left(\frac{0.03\ \text{yr}^{-1}}{R_{\text{SN}}}\right) . \qquad (3.46)$$

On the grounds of the scaling relations we derived for spiral galaxies in Chapters 3.1.2-3, we expect $C \approx 1$ to hold for all spirals. *In fine*, notice that combining the bounds from Eqs.(3.37,3.45) results in all factors containing α', m_{F_1}, m_{F_2} and $|Z'|$ very conveniently cancelling, leaving us with a lower bound on ϵ which does not depend on any other parameter:

$$\epsilon \gtrsim 10^{-10} . \qquad (3.47)$$

The bound above is required to hold in order for the amount of energy converted into dark photons via kinetic mixing induced processes in the core of ordinary supernovae to be sufficiently large as to efficiently heat the halo. This lower bound is consistent with the upper bounds obtained from early Universe cosmology and discussed in Chapter 2. Before we delve further into a study of experimental signatures of this dark matter model, it is beneficial to summarize the constraints we have obtained on the parameter space of our model, whose fundamental physics, the reader will recall, is described by 5 parameters.

---

[8]That is, $R_{\gamma_D} \approx \min\left[\frac{1}{2}\left(\frac{\epsilon}{10^{-9}}\right)^2, \frac{1}{2}\right]$

3.3 Summary of constraints on the model

An essential parameter in terms of new physics is the kinetic mixing parameter, ϵ. A requirement for our dynamical halo model to be viable is that a hefty fraction of the energy output from core-collapse supernovae be converted into the creation of light dark particles (F_1-$\bar{F}_1$ pairs), ultimately reprocessed into dark photons which can heat the halo. This allowed us to determine the lower bound $\epsilon \gtrsim 10^{-10}$ [Eq.(3.47)]. We obtained an upper bound on ϵ by requiring that exotic contributions to the energy density during the radiation dominated era be constrained. Our studies of $\delta N_{\text{eff}}[\text{CMB}]$ and $\delta N_{\text{eff}}[\text{BBN}]$ suggest $\epsilon \lesssim 5 \times 10^{-8}$.

The mass of the lighter of the two particles, m_{F_1}, obeys an upper bound of $\sim 100\,\text{MeV}$, else its pair production mechanism in core-collapse supernovae would be Boltzmann suppressed. Studies of White Dwarfs and Red Giants have instead allowed us to set the lower bound $m_{F_1} \gtrsim 0.01\,\text{MeV}$. Below this value, the allowed region of parameter space for ϵ is in conflict with the lower bound in Eq.(3.47).

In our study of dark recombination, we set bounds on the redshift at which this process took place, requiring that it be greater than the redshift of matter-radiation equality. This requirement in essence means that LSS formation is unaltered by dark acoustic oscillations on scales which are still growing in the linear regime today. We derived useful bounds relating ϵ, m_{F_1} and α' which, along with the limits on ϵ and m_{F_1} discussed above ($10^{-10} \lesssim \epsilon \lesssim 5 \times 10^{-8}$, $0.01\,\text{MeV} \lesssim m_{F_1} \lesssim 100\,\text{MeV}$), indicate the lower bound $\alpha' \gtrsim 10^{-4}$. In addition, our study assumed that we could safely make use of perturbation theory in all our calculations. This of course requires α' to be sufficiently small, and indicatively $\alpha' \lesssim 10^{-1}$.

The heavier of the two particles, F_2, really did enter our dynamics actively only in the context of galactic structure. Recall that when considering energy and entropy transfer between the visible and dark sectors in the early Universe we neglected channels involving F_2 particles on the grounds of the choice $m_{F_2} \gg m_{F_1}$. In relation to dark recombination the crucial quantity in play, that is, the ionization energy of the bound state, was found to not depend on m_{F_2} (once more, provided $m_{F_2} \gg m_{F_1}$). Galactic structure considerations allowed us to obtain constraints on m_{F_2} from two different arguments: the first in relation to the cooling timescale of the dark matter halo, and the second concerning the ionization state of the dark matter plasma. These constraints are given by Eqs.(3.37,3.39,3.45).

The bounds on the 5 fundamental parameters of the model we obtained in this work are interrelated. We present them unitedly below:

$$
\begin{cases}
\epsilon \lesssim \min\left[3.5 \times 10^{-9} \left(\frac{M}{m_e}\right)^{\frac{1}{2}}, \ 10^{-8} \left(\frac{\alpha'}{\alpha}\right)^4 \left(\frac{m_{F_1}}{\text{MeV}}\right)^2 \left(\frac{M}{m_e}\right)^{\frac{1}{2}}\right], \\[2mm]
\epsilon \gtrsim 10^{-10}, \\[2mm]
0.01\,\text{MeV} \lesssim m_{F_1} \lesssim 100\,\text{MeV}, \\[2mm]
m_{F_2} \gtrsim \left(\frac{|Z'|}{10}\right)\left(\frac{\alpha'}{10^{-2}}\right)^2 \left(\frac{m_{F_1}}{\text{MeV}}\right) \text{GeV}, \\[2mm]
m_{F_2} \lesssim \min\left[200 \left(\frac{\text{MeV}}{m_{F_1}}\right)\left(\frac{\alpha'}{10^{-2}}\right)^2 \left(\frac{|Z'|}{10}\right)^{\frac{5}{3}}, \ 100 \left(\frac{|Z'|}{10}\right)^3 \left(\frac{\alpha'}{10^{-2}}\right)^2 \left(\frac{m_{F_1}}{\text{MeV}}\right) g(\alpha', Z')\right] \text{GeV}, \\[2mm]
10^{-4} \lesssim \alpha' \lesssim 10^{-1}, \\[2mm]
|Z'| \gtrsim \max\left[3, 4\left(\frac{m_{F_1}}{10\,\text{MeV}}\right)^3\right].
\end{cases}
\tag{3.48}
$$

At this stage it might be useful to remind the reader that $M \equiv \max(m_e, m_{F_1})$ and $g(\alpha', Z') \equiv \max(\alpha'^3 Z'^4, 1)$. Note that our studies indicate a favoured region of parameter space for the masses of the two fermions, with the lighter (F_1) in the MeV range and the heavier (F_2) in the GeV-TeV range.

CHAPTER 4

EXPERIMENTAL SIGNATURES

4.1 Dark matter shielding radius

Hitherto, our analysis has focused on the phenomenology of this two-fermion dark matter model in the context of early Universe cosmology and galactic structure. Our study has revealed that the favoured scenario is that where the lighter fermion has mass in the MeV range and the heavier in the GeV-TeV range. Two types of interactions, then, are expected to be relevant for direct detection experiments: F_1-electron scattering and F_2-nuclei scattering, while all other types of interactions are kinematically suppressed; for simplicity we will focus exclusively on the latter. Given the self-interacting nature of the dark matter particles, we could expect a number of them to be captured within the Earth and shield the halo dark matter wind. In this Chapter we will determine whether this is the case and, if so, what experimental signatures are expected to be associated. The following analysis will draw from the similar one conducted in the MDM framework in [81].

In the present model, we expect F_2 particles to be captured within the Earth, at first through hard scattering processes. F_2 particles will then pile up in the core of the Earth, and once a significant number have accumulated, dark matter will be captured via self-interaction processes. At this stage a *shielding radius*, R_s, will begin to build up. An F_2 particle which passes through the Earth at a distance $r < R_s$ from the center will then be captured, and hence these particles will accumulate at a rate approximately given by $dN/dt \simeq \pi R_s^2 v_{\rm rot} n_{F_2}$. Once a dark matter particle is captured, it loses energy quickly, decreasing its velocity. In all of this, dark matter particles can also interact with ordinary nuclei via kinetic mixing induced Rutherford scattering; given that the relevant cross-section goes as $d\sigma/d\Omega \sim 1/v^4$, we expect the captured dark matter particles to rapidly thermalize with ordinary matter. It follows that their density [number density] profile $\rho(r)$ [$n_{F_2}(r)$] can be obtained by imposing the hydrostatic equilibrium condition: $dP(r)/dr = -\rho(r)g(r)$. Using local thermal equilibrium to relate P to T via $P = n_{F_2}T$ and by expressing $\rho = m_{F_2}n_{F_2}$, we can express the hydrostatic equilibrium condition as:

$$\frac{dn_{F_2}(r)}{dr} = -\frac{n_{F_2}(r)}{T(r)}\left(m_{F_2}g(r) + \frac{dT(r)}{dr}\right), \tag{4.1}$$

where the local gravitationl acceleration is given by $g(r) = \frac{G}{r^2}\int_0^r dr'\, 4\pi r'^2 \rho_E(r')$.

Solving Eq.(4.1) requires specifying a form for $T(r)$, $\rho(r)$. We do so by adopting a linear approximation for the temperature and density profiles obtained from the Preliminary Reference Earth Model [82]. The profiles $T(r)$, $\rho_E(r)$ are depicted in Figure 4.1. We solve Eq.(4.1) and determine that the number density profile of captured F_2 particles, $n_{F_2}(r)$, depends exclusively on m_{F_2}, and not on the other 4 parameters of our model. Once we have determined the number density profile of the captured F_2 particles, we can estimate the shielding radius following the approach adopted in [81], which we here outline. An F_2 particle is captured when it loses the entirety of its energy. The key quantity in determining whether or not an F_2 particle gets captured is its distance of closest approach to the center of the Earth, $d_{\rm min}$. For a given point in parameter space, there will be a maximum value of $d_{\rm min}$ for which an F_2 particle will be captured: such distance is the shielding radius, R_s.
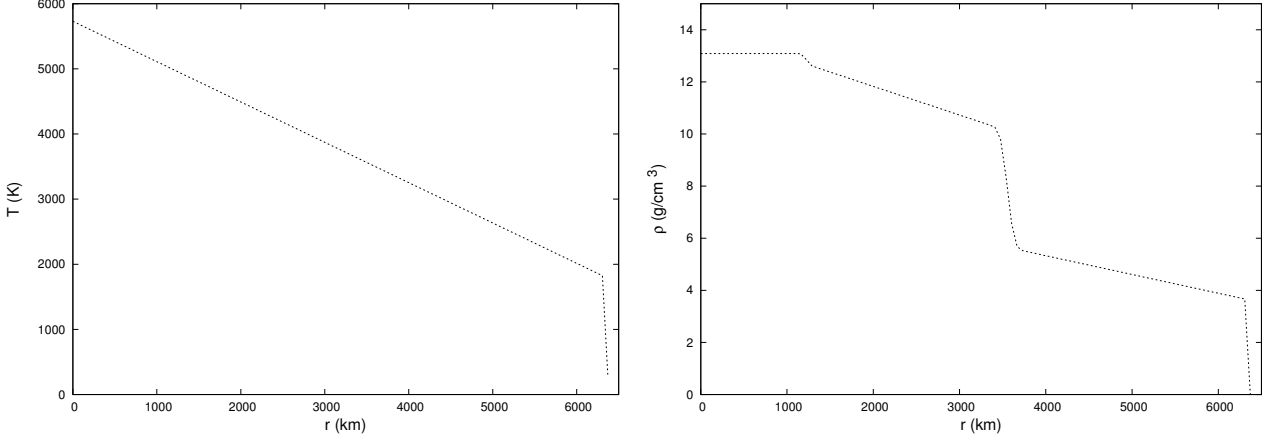
Figure 4.1: Earth's temperature [$T(r)$] and density [$\rho_E(r)$] profiles adopted.

An incoming F_2 particle interacts with the captured F_2 particles via Rutherford scattering, with differential cross-section per recoil energy:

$$\frac{d\sigma}{dE_R} = \frac{2\pi Z'^4 \alpha'^2}{m_{F_2} E_R^2 v^2} \, . \tag{4.2}$$

Consequently, F_2 particles travelling along a path x lose energy at a rate:

$$\frac{dE}{dx} = -n_{F_2}(x) \int_{E_{\min}}^{E_{\max}} dE_R \, E_R \frac{d\sigma}{dE_R} \, , \tag{4.3}$$

where $E_{\max} = m_{F_2} v_{\rm rot}^2/2$ is the maximum kinematically allowed recoil energy and $E_{\min} \simeq m_{F_1}^2 \alpha'^2/(2m_{F_2})$ is determined by the scale at which atomic screening effects start to become relevant. We approximate the trajectories of the F_2 particles by straight lines, along which the distance is traced by the coordinate q; at $r = d_{\min}$, $q = 0$, and the trajectory is symmetric around this point. Imposing that the energy lost equals the initial energy of the F_2 particle, we obtain that an F_2 particle is captured if the following condition is satisfied:

$$\int_{x_i}^{x_f} dx \, n_{F_2}(x) \simeq \int_{q_{\min}}^{q_{\max}} dq \, n_{F_2}(r = \sqrt{d_{\min}^2 + q^2}) \gtrsim \frac{m_{F_2}^2 v_{\rm rot}^4}{16\pi Z'^4 \alpha'^2 \ln\left[\left(\frac{m_{F_2}}{m_{F_1}}\right)\left(\frac{v_{\rm rot}}{\alpha'}\right)\right]} \, , \tag{4.4}$$

where $q_{\max,\min} = \pm\sqrt{R_E^2 - d_{\min}^2}$, and $R_E \simeq 6371$ km is the Earth's radius.

Eq.(4.4) can be solved numerically for a given point in parameter space by looking for the value of $d_{\min}$ for which the right-hand side first exceeds the left-hand side. Our numerical analysis shows that the solution displays a very weak dependence on m_{F_1}, which enters only logarithmically in Eq.(4.4), via the lower limit of the recoil energy integral. Hence, the shielding radius due to dark matter self-interactions in our model depends only on three parameters: m_{F_2}, α' and Z'. We find that the shielding radius today (recall R_s builds up with time) is given by:

$$R_s \simeq \min\left[5300\left(\frac{\alpha'}{10^{-3}}\right)^{0.06}\left(\frac{m_{F_2}}{10\,\text{GeV}}\right)^{-0.55}\left(\frac{|Z'|}{10}\right)^{0.14}\text{km} \, , \, R_E\right] . \tag{4.5}$$

41

4.2 Diurnal modulation signal

The captured dark matter particles can potentially shield the halo dark matter wind, suppressing the rate of interactions with ordinary matter, and hence the signal observed in DDEs. In particular, we will find that, for DDEs located in the Southern hemisphere, this is expected to give rise to an observable diurnal modulation effect. Here a pivotal quantity is the angle between the direction of the Earth's motion through the dark matter halo and the normal vector to the Earth's surface at the relevant detector location, which we denote by ψ. Owing to Earth's rotation around its axis, this angle changes during the day, according to:

$$\cos\psi(t) = \cos\theta_l \sin\left(2\pi\frac{t}{T_d}\right)\sin\langle\theta_h\rangle \pm \sin\theta_l \cos\langle\theta_h\rangle \,. \tag{4.6}$$

Here θ_h is the angle subtended by the Earth's motion through the halo with respect to its spin axis, θ_l denotes the detector latitude, and $T_d \simeq 23.9345$ hrs is the length of a sidereal day. Although θ_h varies slightly during the year due to the Earth's motion around the Sun, we shall not be concerned with such effect and will simply take the average value $\langle\theta_h\rangle \simeq 43°$. In Eq.(4.6) the $+[-]$ sign holds for a detector situated in the Northern [Southern] hemisphere respectively. A value $\psi = 0°$ indicates that the dark matter halo wind is coming vertically down towards the detector; *per contra*, $\psi = 180°$ means that the wind is approaching from the other side of the Earth relative to the detector, hence transiting near the Earth's core, and possibly being captured. The different sign according to the hemisphere in Eq.(4.6) plays a major role, implying that ψ can be as big as $180°$ in the Southern (but not Northern) hemisphere, and hence the diurnal modulation effect is expected to be more pronounced there. In Figure 4.2 we plot the evolution of ψ during one sidereal day for a detector located in the Stawell mine (Victoria, Australia) and one on the Gran Sasso d'Italia (Abruzzo, Italy).
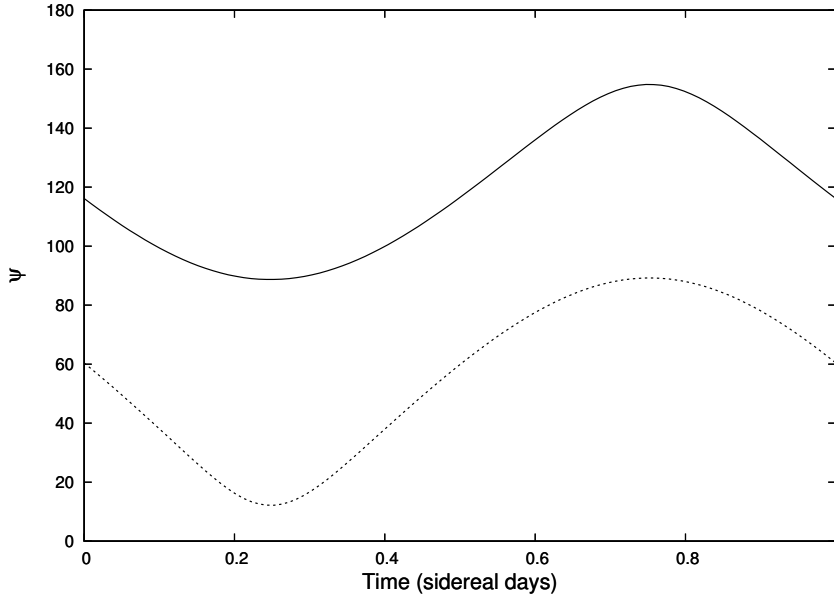

Figure 4.2: $\psi(t)$ at the Stawell mine (solid line) and at Gran Sasso (dashed line).

Defining $\mathbf{v}$ to be the velocity of the halo dark matter particles relative to the Earth (v being its magnitude) and $\mathbf{v}_E$ the velocity of the Earth relative to the galactic halo ($|\mathbf{v}_E| \simeq 220$ km/s), the interaction rate of dark matter particles with the target atoms in the detector depends on the quantity (see e.g. [81]):

$$\mathcal{I} \equiv \int_0^{2\pi} d\phi \int_{-1}^1 d\theta \, \sin\theta \int_{v_{\min}}^\infty dv \, v e^{-\frac{(\mathbf{v}+\mathbf{v}_E)^2}{v_0^2}} \,. \tag{4.7}$$

Here $v_0^2 = v_{\text{rot}}^2 \overline{m}/m_{F_2} = 2\sigma_{F_2}^2/3$, σ_{F_2} being the velocity dispersion of the F_2 particles and $v_{\text{min}} = \sqrt{(m_T + m_{F_2})^2 E_R/(2 m_T m_{F_2}^2)}$ is a lower limit determined by kinematics. The mass of the target atoms is m_T and E_R is the recoil energy at which we wish to investigate the modulation effect. Shielding is accounted for by modifying the integral in Eq.(4.7), as in [81], as follows:

$$\mathcal{I}[\psi(t)] = \mathcal{I} \equiv \int_0^{2\pi} d\phi \int_{-1}^1 d\theta \, \sin\theta \int_{v_{\text{min}}}^\infty dv \, v e^{-\frac{(\mathbf{v}+\mathbf{v}_E)^2}{v_0^2}} H[d_{\text{min}}(\theta, \phi, \psi) - R_s] \,, \tag{4.8}$$

where we have multiplied the integrand of Eq.(4.7) by a Heaviside step function, which is itself a function of the distance of closest approach, d_{min}, given by:

$$d_{\text{min}} = \begin{cases} R_E \sqrt{1 - g^2(\theta, \phi, \psi)}, & \text{if } g(\theta, \phi, \psi) \geq 0 \,, \\ R_E, & \text{if } g(\theta, \phi, \psi) < 0 \,, \end{cases} \tag{4.9}$$

having defined $g(\theta, \phi, \psi) \equiv \sin\theta \sin\phi \sin\psi - \cos\theta \cos\psi$. We can now compute $\mathcal{R}$, the percentage rate suppression due dark matter capture ($\mathcal{R} = 100\%$ indicates a total suppression):

$$\mathcal{R} = 100 \left(1 - \frac{\mathcal{I}[\psi(t)]}{\mathcal{I}} \right) \%, \tag{4.10}$$

Of course, the value of interest here is $\mathcal{R}_{\text{max}}$, the maximum percentage rate suppression during the course of a sidereal day, since we wish to observe an *all or nothing* outcome. We investigate this effect only for detectors located in the Southern hemisphere since, for detectors located in the Northern hemisphere, $\mathcal{R}_{\text{max}}$ is typically small ($\lesssim 10\%$), so we do not expect such effect to be observable in the near future. No dark matter experiments have been conducted in the Southern hemisphere yet, although two are being planned: the first in the Stawell mine (near Melbourne, $\theta_l \simeq 37.1°$), and the second in the Andes Lab (on the Argentinean-Chilean border, $\theta_l \simeq 30.7°$). In Figure 4.3 we plot $\mathcal{R}$ for a detector located at the Stawell mine versus time over the duration of a sidereal day, for some example parameter choice. Numerically, we find that the maximum percentage rate suppression is to very good approximation independent of the recoil energy (within the range $0.1 \text{ keV} \lesssim E_R \lesssim 20 \text{ keV}$) and of the target mass, depending exclusively on α', m_{F_2} and $|Z'|$. For a detector located at the Stawell mine, the maximum percentage suppression rate is found to be:[1]

$$\mathcal{R}_{\text{max}} \simeq \min \left[55 \left(\frac{\alpha'}{10^{-3}} \right)^{0.1} \left(\frac{m_{F_2}}{50 \text{ GeV}} \right)^{-0.9} \left(\frac{|Z'|}{10} \right)^{0.6} \% \,, 100\% \right] \,. \tag{4.11}$$

4.3 Prospects for direct & indirect detection and collider production

As we mentioned at the outset of the Chapter, two types of interactions are of notable interest in the context of DDEs within the framework of our model. That is, F_1-electron and F_2-nuclei scattering, with other interactions being kinematically suppressed. Previous work had found that spin-independent elastic F_2-nuclei scattering could explain both the positive and negative results arising from direct detection experiments consistently, provided $\epsilon \sim 10^{-9}$ [43]. Then came LUX [44], bringing with her[2] the negative search results which now

---

[1] For a detector located at the Andes Lab, simply replace the number "55" in Eq.(4.11) with "40".
[2] In Latin, the word "lux" (pronounced "loox"), which means "light", is feminine.
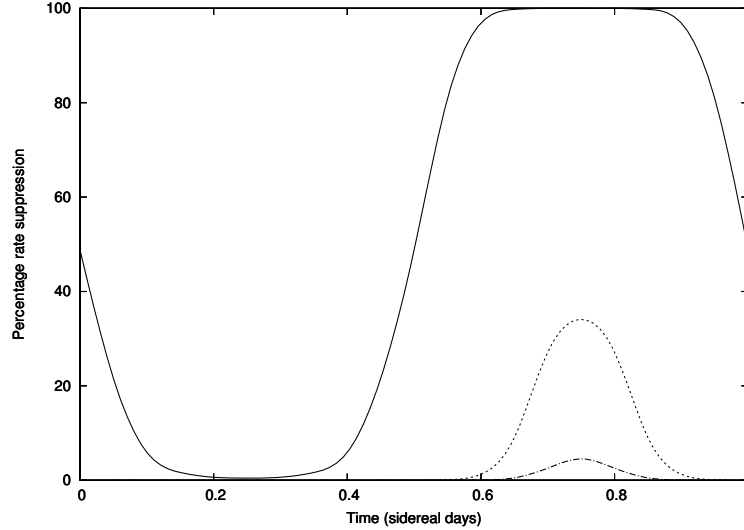
Figure 4.3: Percentage suppression rate for detectors situated at the Stawell mine for m_{F_2}=10 GeV, 100 GeV, 1 TeV (solid, dashed, dot-dashed line). We have assumed $\alpha' = 10^{-2}$, $|Z'| = 10$, a recoil energy of 2 keV and an Na target ($m \simeq 23 m_p$).

mean that an explanation of the DAMA annual modulation signal [83] in terms of nuclear recoils is strongly disfavoured. Recent work within the MDM framework has shown that it is still possible to explain the DAMA annual modulation signal in terms of a dark matter particle with mass in the MeV range scattering off electrons [84]. In the framework of our model we can then interpret the annual modulation signal observed by DAMA in terms of F_1-electron scattering, which could also explain the modulation observed by CoGeNT at low recoil energies [85], and has the potential to be probed by large Xenon experiments such as LUX [44] and XENON100 [86].

The prospects of producing F_1 or F_2 particles in colliders such as the LHC through kinetic mixing induced processes are not the most promising. A rough calculation reveals that for an integrated luminosity of ~ 25 fb^{-1}, at $\sqrt{s} = 10$ TeV, the expected number of events for a process of the type SM+SM→DM+DM (where "SM" and "DM" denote Standard Model and dark matter particles respectively), with cross-section $\sigma \sim \epsilon^2 \alpha^2/s$, is about 10^{-16} for $\epsilon \sim 10^{-9}$! The $1/s$ dependence of the cross-section, which follows from the masslessness of the mediator (the photon), implies that raising $\sqrt{s}$ will not improve things in this respect. It is still possible to produce these particles in colliders if we introduce additional interactions which we have not considered in this thesis, for instance a Higgs portal coupling.

We briefly comment on possible indirect detection signals. As emphasized at the start, our model is an example of asymmetric dark matter, where the relic abundances are set by a particle-antiparticle asymmetry. In the early Universe, annihilation processes of the type $F_j \overline{F}_j \rightarrow \gamma_D \gamma_D$, with cross-section $\sigma_{\text{ann}} \propto \alpha'^2/m_{F_j}^2$, are expected to efficiently annihilate the symmetric components of the F_j particles. It is possible that for the heavier of the two particles, F_2, the annihilation rate might not be sufficiently high, so that we might end up with a symmetric relic abundance of F_2 and $\overline{F}_2$ on top of the asymmetric one. Given the approach we adopted, that is, having started with $\mathcal{X} = T_{\gamma_D}/T_\gamma = 0$ at early times, with $\mathcal{X}$ (and hence the dark matter particles) subsequently generated via kinetic mixing induced processes, such a scenario is certainly unlikely, but still possible. Should there indeed be a leftover symmetric F_2 component, we expect potential annihilation processes and hence indirect detection signals. In [87] the reader will find more information on direct and indirect detection of dissipative dark matter. For a recent study on annihilation signals from asymmetric dark matter, we refer the reader to [88].

44

CHAPTER 5

CONCLUSIONS

Even as these lines are being written, the origin and composition of the mysterious dark matter which appears to pervade the Universe remains obscure. Although a multitude of dark matter candidates have emerged from the most diverse frameworks, a compelling dark matter theory has yet to be formulated. A number of astrophysical observations suggest that, despite it performing magnificently on large scales, our current understanding of collisionless cold dark matter suffers from a series of drawbacks on small scales. In fact, such discrepancies might well be overtly pointing towards the need for a shift from the collisionless cold dark matter paradigm towards, for instance, self-interacting dark matter.

From a particle physics mindset, a well motivated means of incorporating dark matter is by appending a hidden sector to the Standard Model. Arguably, the simplest choice in this respect is that of a hidden sector featuring a $U(1)$ gauge symmetry, whose interactions are mediated by a dark photon. This thesis has made a contribution to the vast literature already present on this class of theories, by examining one where the entire dark matter content is subject to sizeable dissipative interactions. The model considered features two charged fermions and a dark photon which interacts via kinetic mixing with the ordinary photon. In Chapter 2 we employed cosmological constraints on the energy density during the radiation epoch to set bounds on the parameter space of the model.

Perhaps the most interesting part of our work was the one carried out in Chapter 3, where we analysed this same model in the context of galactic structure. The dissipative nature of the interactions mediated by the dark photon, which would make the dark matter halo cool, calls for a heat source which can replace the energy lost. We found that kinetic mixing induced processes arising within the core of ordinary supernovae can inject the required heat, provided $\epsilon \sim 10^{-9}$. Under the assumption that the dark matter galactic halo reaches a static configuration, with the heating and cooling rates matching at each point in the halo, we have shown that a series of unexplained scaling relation observed to hold for spiral galaxies (chief among them the Tully-Fisher relation) all follow rather straightforwardly from this energy balance condition.

A theoretical model is useless if it is not testable. In Chapter 4 we have expounded how the self-interacting nature of this dark matter gives rise to an unique signature: a diurnal modulation in the rate of interactions of the heavier dark fermion with nuclei in direct detection experiments. This effect could be successfully exploited as a probe of the present and other self-interacting dark matter models via, for instance, direct detection experiments located in the Southern hemisphere.

Dissipative dark matter is an unconventional choice of dark matter candidate. Notwithstanding the general inclination, we have demonstrated that it is not only a possibility, but a rich and interesting one for that matter. It has the potential to allow us to elegantly bridge the gap between theory and astronomical observations, and address a number of worrisome shortcomings of collisionless cold dark matter. Given the *status quo* of confusion with respect to direct detection experiments we are experiencing, a deeper understanding of these astronomical observations could be a key to unraveling the puzzle of dark matter, and further our understanding of its nature. Dark matter first appeared to us in the skies. Perhaps, then, it is in the blue expanse that we should seek to better comprehend the mystery of its origin.

APPENDIX A

WHY CAN DARK THOMSON SCATTERING BE NEGLECTED?

In this Appendix we argue that, for $m_{F_1} \gtrsim 0.1$ MeV, dark Thomson scattering is an inefficient heating mechanism, and hence uphold our approach of solely considering dark photoionization. Recall, dark Thomson scattering consists of the process $\gamma_D F_1 \to \gamma_D F_1$, where F_1 denotes a free F_1 particle. The cross-section for dark Thomson scattering is:

$$\sigma_{DT} = \frac{8\pi}{3} \frac{\alpha'^2}{m_{F_1}^2} . \tag{A.1}$$

Making use of the relation between the free F_1 number density and the dark matter density profile, that is, $n_{F_1} = \rho\kappa(|Z'| - 2)$, we obtain the optical depth for dark Thomson scattering considering a photon which propagates from the galactic center to infinity being:

$$\tau = \int_0^\infty dr\, \sigma_{DT} n_{F_1} = \int_0^\infty dr\, \sigma_{DT} \rho\kappa(|Z'| - 2) = \frac{4\pi^2 \alpha'^2 \kappa(|Z'| - 2)\rho_0 r_0}{3m_{F_1}^2} . \tag{A.2}$$

If we assume that the spectrum of dark photons heating the halo peaks significantly below m_e, simple kinematic considerations imply that the only way for dark Thomson scattering to be able to efficiently impart energy to the scattered particle is if $\tau \gg 1$, that is, if the dark photon remains trapped in the galaxy. Using the expression above for the optical depth, this translates to:

$$m_{F_2} \ll \frac{4\pi^2 \rho_0 r_0 \alpha'^2 |Z'|}{3m_{F_1}^2} , \tag{A.3}$$

where we have used $\kappa \approx 1/m_{F_2}$. Recall we obtained a lower bound on the mass of the F_2 particle by requiring that the halo be ionized [Eq.(3.39]. If we impose that the upper bound obtained above be greater than the lower bound in question, we find this gives us the following condition on the mass of the F_1 particle:

$$m_{F_1}^3 \ll \frac{4\pi^2 \rho_0 r_0 v_\infty^2 \xi_{\max}}{3} , \tag{A.4}$$

where recall $\xi_{\max} \approx 7 - 28$. We find that Eq.(A.4) reduces to:

$$\frac{m_{F_1}}{\text{MeV}} \ll \left(\frac{\rho_0 r_0}{100 \, \frac{M_\odot}{\text{pc}^2}} \right)^{\frac{1}{3}} \left(\frac{v_\infty}{300 \, \frac{\text{km}}{\text{s}}} \right)^{\frac{2}{3}} . \tag{A.5}$$

The above is the *conditio sine qua non* for dark Thomson scattering to be an important heating mechanism. For this to not be the case for all spirals ($v_\infty \lesssim 300$ km/s), we then find that $m_{F_1} \gtrsim 0.1$ MeV is required, as anticipated.

[1] R. Foot and S. Vagnozzi. *Phys.Rev.*, D91(2):023512, 2015.

[2] R. Foot and S. Vagnozzi. arXiv:1412.0762 [hep-ph].

[3] F. Zwicky. *Helv.Phys.Acta*, 6:110–127, 1933.

[4] V. C. Rubin and W. K. Jr. Ford. *Astrophys.J.*, 159:379–403, 1970.

[5] E. Komatsu et al. *Astrophys.J.Suppl.*, 192:18, 2011.

[6] S. Dodelson. *Modern cosmology*. 2003.

[7] Y.B. Zeldovich. *Astron.Astrophys.*, 5:84–89, 1970.

[8] A. Refregier. *Ann.Rev.Astron.Astrophys.*, 41:645–668, 2003.

[9] P.A.R. Ade et al. *Astron.Astrophys.*, 2014.

[10] K. Garrett and G. Duda. *Adv.Astron.*, 2011:968283, 2011.

[11] J. F. Navarro, C. S. Frenk, and S. D.M. White. *Astrophys.J.*, 462:563–575, 1996.

[12] W.J.G. de Blok. *Adv.Astron.*, 2010:789293, 2010.

[13] A. A. Klypin, A. V. Kravtsov, O. Valenzuela, and F. Prada. *Astrophys.J.*, 522:82–92, 1999.

[14] S.F. Novaes. *Standard Model: An Introduction*, arXiv:0001283 [hep-ph]. 1999.

[15] J. L. Feng. *Ann.Rev.Astron.Astrophys.*, 48:495–545, 2010.

[16] S. Profumo. arXiv:1301.0952 [hep-ph]. 2013.

[17] S. P. Martin. *Adv.Ser.Direct.High Energy Phys.*, 21:1–153, 2010.

[18] J. R. Ellis et al. *Nucl.Phys.*, B238:453–476, 1984.

[19] R.D. Peccei and H. R. Quinn. *Phys.Rev.Lett.*, 38:1440–1443, 1977.

[20] H. Goldberg and L. J. Hall. *Phys.Lett.*, B174:151, 1986.

[21] J. L. Feng, M. Kaplinghat, H. Tu, and H. Yu. *JCAP*, 0907:004, 2009.

[22] K. Petraki, L. Pearce, and A. Kusenko. *JCAP*, 1407:039, 2014.

[23] S. Andreas, Mark D. Goodsell, and A. Ringwald. *AIP Conf.Proc.*, 1563:114–117, 2013.

[24] D. E. Kaplan, G. Z. Krnjaic, K. R. Rehermann, and C. M. Wells. *JCAP*, 1005:021, 2010.

[25] J. M. Cline, Z. Liu, and W. Xue. *Phys.Rev.*, D85:101302, 2012.

[26] F. Cyr-Racine and K. Sigurdson. *Phys.Rev.*, D87(10):103515, 2013.

[27] D. N. Spergel and P. J. Steinhardt. *Phys.Rev.Lett.*, 84:3760–3763, 2000.

[28] J. Fan, A. Katz, L. Randall, and M. Reece. *Phys.Rev.Lett.*, 110(21):211302, 2013.

[29] R. Foot, H. Lew, and R.R. Volkas. *Phys.Lett.*, B272:67–70, 1991.

[30] R. Foot. *Int.J.Mod.Phys.*, A29:1430013, 2014.

[31] R. Foot and X. He. *Phys.Lett.*, B267:509–512, 1991.

[32] B. Holdom. *Phys.Lett.*, B166:196, 1986.

[33] R. Foot. *Phys.Lett.*, B718:745–751, 2013.

[34] P. Ciarcelluti and R. Foot. *Phys.Lett.*, B679:278–281, 2009.

[35] R. Foot. *Phys.Lett.*, B711:238–243, 2012.

[36] R. Foot and R.R. Volkas. *Phys.Rev.*, D70:123508, 2004.

[37] G.G. Raffelt. *Stars as laboratories for fundamental physics*. 1996.

[38] R. Foot. *arXiv:1307.1755 [astro-ph]*. .

[39] R. Foot. *Phys.Lett.*, B728:45–50, 2014.

[40] K. Petraki and R. R. Volkas. *Int.J.Mod.Phys.*, A28:1330028, 2013.

[41] K. M. Zurek. *Phys.Rept.*, 537:91–121, 2014.

[42] N. F. Bell, K. Petraki, I. M. Shoemaker, and R. R. Volkas. *Phys.Rev.*, D84:123505, 2011.

[43] R. Foot. *Phys.Rev.*, D88(2):025032, 2013.

[44] D.S. Akerib et al. *Phys.Rev.Lett.*, 112:091303, 2014.

[45] J. M. Cline, Z. Liu, G. Moore, and W. Xue. arXiv:1312.3325 [hep-ph].

[46] J. Bernstein, M. Ruderman, and G. Feinberg. *Phys.Rev.*, 132:1227–1233, 1963.

[47] J. R. Ellis and K. A. Olive. *Nucl.Phys.*, B223:252, 1983.

[48] M.I. Dobroliubov and A. Yu. Ignatiev. *Phys.Rev.Lett.*, 65:679–682, 1990.

[49] S. Davidson, B. Campbell, and D. C. Bailey. *Phys.Rev.*, D43:2314–2321, 1991.

[50] S. Davidson, S. Hannestad, and G. Raffelt. *JHEP*, 0005:003, 2000.

[51] R. Foot, A. Kobakhidze, K. L. McDonald, and R. R. Volkas. *Phys.Rev.*, D89:115018, 2014.

[52] E. W. Kolb, D. Seckel, and M. S. Turner. *Nature*, 314:415–419, 1985.

[53] H.M. Hodges. *Phys.Rev.*, D47:456–459, 1993.

[54] Z.G. Berezhiani, A.D. Dolgov, and R.N. Mohapatra. *Phys.Lett.*, B375:26–36, 1996.

[55] H. Vogel and J. Redondo. *JCAP*, 1402:029, 2014.

[56] E. D. Carlson and S.L. Glashow. *Phys.Lett.*, B193:168, 1987.

[57] D. Binosi and L. Theul. *Computer Physics Communications*, 161(1-2):76–86, 2004.

[58] E. W. Kolb and M. S. Turner. *The Early Universe. Front.Phys.*, 69:1–547, 1990.

[59] P. Gondolo and G. Gelmini. *Nucl.Phys.*, B360:145–179, 1991.

[60] J. Dunkley et al. *Astrophys.J.*, 739:52, 2011.

[61] R. Keisler et al. *Astrophys.J.*, 743:28, 2011.

[62] S. Weinberg. *Cosmology*. 2008.

[63] J. Bernstein, L. S. Brown, and G. Feinberg. *Rev.Mod.Phys.*, 61:25, 1989.

[64] Y.I. Izotov and T.X. Thuan. *Astrophys.J.*, 710:L67–L71, 2010.

[65] K. Petraki, M. Trodden, and R. R. Volkas. *JCAP*, 1202:044, 2012.

[66] Z. Berezhiani, D. Comelli, and F. L. Villante. *Phys.Lett.*, B503:362–375, 2001.

[67] A. Y. Ignatiev and R.R. Volkas. *Phys.Rev.*, D68:023518, 2003.

[68] J. Beringer et al. *Phys.Rev.*, D86:010001, 2012.

[69] D. Maoz. *Astrophysics in a nutshell*. Princeton Univ. Press, Princeton, NJ, 2007.

[70] M. Schmidt. *Astrophys.J.*, 129:243, 1959.

[71] G. B. Rybicki and A. P. Lightman. *Radiative Processes in Astrophysics*. Wiley, 1979.

[72] K.C. Freeman. *Astrophys.J.*, 160:811, 1970. doi: 10.1086/150474.

[73] F. Donato and P. Salucci. *Mon.Not.Roy.Astron.Soc.*, 353:L17–L22, 2004.

[74] W. Li et al. arXiv:1006.4613 [astro-ph]. 2010.

[75] R. L. Webster et al. *Mon.Not.Roy.Astron.Soc.*, 391:1712–1728, December 2008.

[76] J. Kormendy and K.C. Freeman. *ASP Conf.Ser.*, 2004.

[77] F. Shankar et al. *Astrophys.J.*, 643:14–25, 2006.

[78] P. Salucci et al. *Mon.Not.Roy.Astron.Soc.*, 378:41–47, 2007.

[79] S.M. Faber and R.E. Jackson. *Astrophys.J.*, 204:668, 1976.

[80] G. Gentile, P. Salucci, U. Klein, and G. L. Granato. *Mon.Not.Roy.Astron.Soc.*, 375:199–212, 2007.

[81] R. Foot. *JCAP*, 1204:014, 2012.

[82] A. M. Dziewonski and D. L. Anderson. *Phys. Earth Planet. Interiors*, 25:297–356, 1981.

[83] R. Bernabei et al. *Eur.Phys.J.*, C73:2648, 2013.

[84] R. Foot. arXiv:1407.4213 [hep-ph]. .

[85] C.E. Aalseth et al. *Phys.Rev.Lett.*, 107:141301, 2011.

[86] E. Aprile et al. *Phys.Rev.Lett.*, 109:181301, 2012.

[87] J. Fan, A. Katz, and J. Shelton. *JCAP*, 1406:059, 2014.

[88] N. F. Bell, S. Horiuchi, and I. M. Shoemaker. arXiv:1408.5142 [hep-ph]. 2014.